

國立交通大學

光電工程學系
顯示科技研究所

碩士論文

分區場序列式全彩液晶顯示器
背光模組之研究



**Study on Localized Light Pipe for Field –
Sequential – Color LCD Backlight System
Application**

研究生：簡銘進

指導教授：田仲豪 博士

中華民國九十六年七月

分區場序列式全彩液晶顯示器
背光模組之研究

**Study on Localized Light Pipe for Field –
Sequential – Color LCD Backlight System
Application**

研究生：簡銘進
指導教授：田仲豪

Student: Ming-Chin Chien
Advisor: Dr. Chung-Hao Tien



Submitted to Display Institute & Photonic Department
College of Electrical Engineering Science
National Chiao-Tung University
in Partial Fulfillment of the Requirements
for the Degree of Master
In
Display Institute
July 2007
Hsin-Chu, Taiwan, Republic of China.

中華民國九十六年七月

致謝

首先要感謝我指導教授田仲豪老師這幾年來在研究上、表達能力及生活細節上無私的細心指導，並且提供我們良好的研究環境，使我在碩士生涯對於光學原理與背光系統有深入的了解，並順利完成本論文。

實驗室的日子裡，首先要感謝陳永志與蘇志揚同學及林國楠在各方面的合作與協助，還有鄭璧如學姊、姚柏宏、李企桓學長在研究過程提供許多寶貴的建議，同時還要感謝其他學長姊、同學和學弟在課業上、生活上、研究上的幫助與分享，並陪伴我一起度過這些快樂的日子。

此外，我要感謝和工研院機械所林宗信、黃萌祺先生，在研究期間提供我實驗材料以及技術上的協助，讓我實驗得以順利完成。

最後，對於我的父母、哥哥、姐姐及女友，我要感謝你們多年來的支持與鼓勵，還有生活上的細心照顧與關懷，使我能夠無後顧之憂的研究與學習，並順利完成碩士學業。這份喜悅我將與幫助過我的各位分享。



分區場序列式全彩液晶顯示器 背光模組之研究

研究生：簡銘進

指導教授：田仲豪 博士

國立交通大學
光電工程學系 顯示科技研究所

摘要

本篇論文主要目的為對光導管做一分析與研究，特別是為了應用於小尺寸分區場序列式液晶顯示器背光模組。場序式掃描為背光系統提供一種不需使用彩色濾光片及達到高效能高色彩飽和的方法。光源由光導管入光面射入，於其中傳播，當全內反射條件不滿足時便會出射，其不滿足全內反射原因可能為光導管本身形狀或是光接觸到一些微結構時會改變原有行進方向。光導管的設計於背光的應用上有其應遵守的一些規範，除每一區塊的均勻度需有符合人眼所能接受的範圍，我們利用一光準直元件與光導管底部微結構控制出光發散角及分區間的漏光現象，以達到最後顯示的色彩無色偏現象。並經由模擬與實作來實現我們對於小尺寸分區場序式的背光設計。


Study on Localized Light Pipe for Field – Sequential – Color LCD Backlight System Application

Student: Ming-Chin Chien

Advisor: Dr. Chung-Hao Tien

**Department of Photonics & Display Institute
National Chiao Tung University**

Abstract

The logo of National Chiao Tung University is a circular emblem. It features a gear-like outer border. Inside the circle, there is a stylized representation of a book and a pen, with the acronym 'NCTU' and the year '1896' prominently displayed.

The aim of this thesis is to analyze and investigate the light pipe principle, especially for that applied to the small size field-sequential color liquid crystal display. The field-sequential scanning backlight system has a lot of advantages such as high efficiency, high color gamut, and colorfilter-less. When the light coupled into the pipe, the ray propagates inside the pipe under a cone of aperture and then reflected outside the pipe by the micro structure deposited on the bottom or the shape of the pipe itself. The design of the pipe should have some criteria. For example, the non-uniformity should not be noticed by human eye and divergence angle should be well controlled. The light-collimating bars and the light pipes were adapted to manage the light illuminating angle and the light leakage into the other section in order to display the correct color on the panel. Through the simulation and experiment, a backlight for the small size field-sequential color liquid crystal display has been realized.

Table of Contents

Abstract (Chinese)

Abstract (English)

Table of Contents

Figure Caption

<i>Chapter 1 Introduction</i>	<i>1</i>
1.1 Field-Sequential-Color Crystal Display (FSC LCD).....	3
1.2 Scanning Backlights Application to FSC LCD.....	5
1.3 Motivation and Objective of this Thesis.....	7
1.4 Organization of this Thesis.....	7
<i>Chapter 2 Principle of Illumination Light Pipes</i>	<i>8</i>
2.1 Victor Form of Ray-Tracing Equation.....	8
2.1.1 Refraction Law.....	8
2.1.2 Reflection Law.....	9
2.2 Fresnel Reflection.....	10
2.2.1 Reflection Coefficients.....	10
2.2.2 Typical Reflectance of Dielectric Media.....	11
2.2.3 Typical Reflectance of Metal.....	12
2.2.4 Reflectance of the Pipe-Air-Metal Interface.....	13
2.3 Radiometry and Photometry Quantities.....	15
2.3.1 Radiometry.....	15
2.3.2 Photometry.....	17
2.4 The Light Pipe Concept.....	18

2.4.1	Variable Cross Section Light Pipe.....	19
2.4.2	Refractive and Reflective Outcouplers.....	21
<i>Chapter 3 Simulations and Discussions</i>		24
3.1	Introduction.....	24
3.2	Simulation Tool.....	24
3.3	Simulation Model of FSC LCD Backlight System.....	24
3.4	The Determination for the Type of the Micro Structure.....	27
3.5	Optimization of FSC LCD Backlight System.....	29
3.5.1	Optimization of the light-collimating bars.....	29
3.5.2	Optimization of the linear light pipe.....	30
3.6	Summary.....	36
<i>Chapter 4 Experimental Results and Discussion</i>		37
4.1	Introduction.....	37
4.2	Light Source Properties.....	38
4.3	Micro-groove profiles.....	39
4.4	Optical Performances.....	40
4.5	Summary.....	43
<i>Chapter 5 Conclusions &Future works</i>		45
<i>Reference</i>		47



Figure Caption

[Fig. 1.1] Example of light pipe illumination system.....	1
[Fig. 1.2] CIE color space diagram.....	4
[Fig. 1.3] Timing chart for multi-flashing method.....	5
[Fig. 1.4] The results of color image. (a) Light guide without partition. (b) Light guide partitioned into linear light pipes.....	7
[Fig. 2.1] Representation of Snell's law in the plane of incidence.....	8
[Fig. 2.2] Derivation of the vectorial law of refraction.....	9
[Fig. 2.3] Derivation of the vectorial law of reflection.....	10
[Fig. 2.4] Fresnel reflection/refraction.....	11
[Fig. 2.5] Transmittance and Reflectance for $n_1 = 1.0$, and $n_2 = 1.5$	12
[Fig. 2.6] Transmittance and Reflectance for $n_1 = 1.5$, and $n_2 = 1.0$	12
[Fig. 2.7] Reflectance of Au, Al, and Ag for $n_1 = 1.0$	13
[Fig. 2.8] Reflectance of Au, Al, and Ag for $n_1 = 1.5$	13
[Fig. 2.9] Parameters of the pipe-reflector configuration.....	14
[Fig. 2.10] Reflectance of the pipe surrounded by an Al reflector.....	15
[Fig. 2.11] schematic diagram of projection area.....	16
[Fig. 2.12] Simple radiometry problem.....	17
[Fig. 2.13] Human visual response function.....	18
[Fig. 2.14] (a) Linear light pipe. (b) Circular light pipe. (c) Plate light pipe.....	19
[Fig. 2.15] Discontinuous variable cross-section light pipe.....	19
[Fig. 2.16] The equivalent modal for the light propagate in the wedge light pipe.....	21
[Fig. 2.17] Example of refractive outcoupling case.....	21
[Fig. 2.18] Outcoupling angles achieved by refraction for different orientations of the refractive surface.....	22
[Fig. 2.19] Outcoupling produced by a reflective micro-prism.....	23

[Fig. 2.20] Outcoupling angles achieved by reflection for different orientations of the reflective micro-prism.....	23
[Fig 3.1] Schematic diagram of the proposed backlight system.....	24
[Fig 3.2] The repartition of the flux at different positions inside the clear light pipe..	26
[Fig 3.3] (a) Angular light distribution measured on a bare linear light guide with uniformly positioned micro-prisms on the front and gradationally positioned micro-prisms on the rear. (b) Angular light distribution on a bare linear light guide with micro-reflector array on the rear.....	27
[Fig 3.4] The all radiated light from double prism (Mode1 is the radiated light from the sub prism and Mode2 is the radiated light from the main prism).....	28
[Fig 3.5] The wedge-type light pipe needs the TIR prism sheet to modify the illumination light.....	28
[Fig. 3.6] The zones of light-collimating bar.....	29
[Fig 3.7]The angular distribution of the extraction light from light-collimating bar.....	30
[Fig 3.8] The parameters of the micro-groove structure.....	30
[Fig 3.9] The optimization flow chart.....	31
[Fig 3.10] The angular distribution simulated under the various groove orientations.	32
[Fig 3.11] Encoding schemes of (a) modulating frequency and (b) varying groove size.....	32
[Fig 3.12] Near-field discontinuities.....	33
[Fig 3.13] Illumination map of light guide plates with a single division lit up.....	34
[Fig 3.14] The relation between the groove width and the Z-axis position.....	34
[Fig 3.15] Illumination map of light guide plates with a single division lit up.....	35
[Fig 3.16] Rectangular candela distribution plot for divergence of light extraction on the x-y and y-z plane, respectively.....	35

[Fig 3.17] Illumination map of light guide plates with a single division lit up.....	36
[Fig. 4.1] FSC LCD backlight system.....	37
[Fig. 4.2] Angular distribution of the 3-in-1 LED (a) Red (b) Green (c) Blue light...39	39
[Fig. 4.3] The micro-groove profiles measured under the optical microscope.....	39
[Fig. 4.4] The micro-groove profiles measured under the alpha step.....	39
[Fig 4.5] The angular distribution of the extraction light measured at different positions on the light guide output surface.....	41
[Fig 4.6] The sixteen points measurement for the illumination map of light guide plates with a single division lit up.....	43

Table Caption

[Table 1.1] List of publications related to light pipe.....	2
[Table 1.2] Requirements for the backlight unit.....	6
[Table 2.1] Energy-based Units.....	16
[Table 2.2] Photometric Quantities.....	18
[Table 3.1] The specification of the desired prototype FSC LCD.....	26

Chapter 1

Introduction

Introduction

Light pipes are already widely-used components for all kinds of electro-optical systems, like projector, [1] backlight systems for liquid crystal display (LCD), [2] optical mouse, and automotive dashboard. [3]-[4] Therefore, light pipes have turn into critical elements in a variety of applications. In this thesis the analysis and development for the illumination light pipe applied to field-sequential color (FSC) LCD backlight system will be given. Light pipes, like optical fibers, are solid tubes typically made of plastic such as Acrylic or PMMA. However, unlike optical fibers they do not have any type of cladding. Plastic light pipes offer a relatively inexpensive and simple fabrication process, ex. Injection-Moulding, for lighting and illumination purpose. Light pipe illumination systems collect light from a light source, transport the light to a desired location, and output coupled light to illuminate a display. [Fig.1.1] shows an example of a light pipe illumination system for backlight and automotive display.

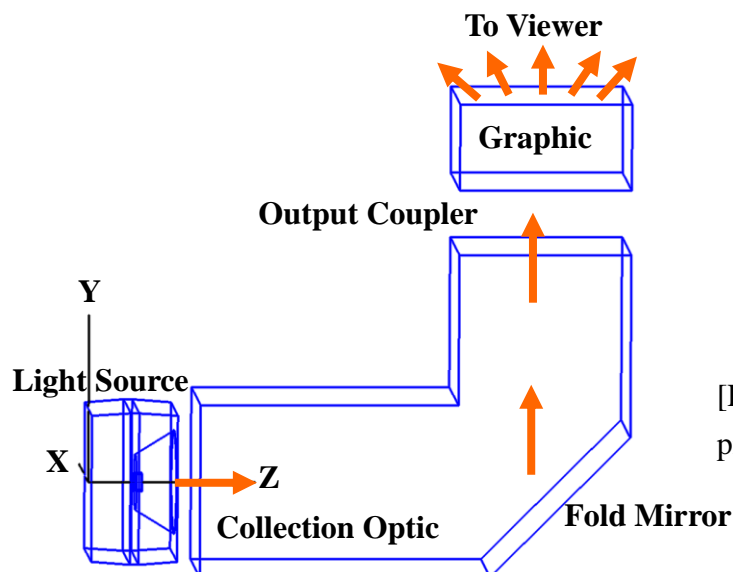


[Fig. 1.1] Example of light pipe illumination system

Recently, there are a number of researches related to the design of light pipe in the published literatures. Gupta et al. presented the concept of principal sections of a light pipe to analyze the propagation of light through the light pipe by total internal reflection (TIR). The acceptance angle and the regions where the leakage occurs first are only determined by the principle section. [5] An analytical modal, termed the flux confinement diagram (FCD), developed by Derlofske et al. was to describe the flux input coupling, transport, and output coupling in light pipe illumination systems. [6] S. Chu and J. Chern demonstrated no-loss bent light pipes with an equiangular spiral. [7] Y. Cheng and J. Chern analytically and numerically investigated, the irradiance formation of an asymmetrically located Lambertian light source in hollow straight light pipes with square and circular shapes. [8] Davenport et al. took a fresh look at some angle-to-area conversion linear light pipes. [9] Koshel and Gupta developed a set of parameters to describe the overall shape of an in-plane light pipe section. [10] All of these literatures established some essential and major concepts about how we can design the light pipe and how the light propagates in it. The following is a list of the relevant references of the light pipes, shown in [Table 1.1]. [5]-[10]

[Table 1.1] List of publications related to light pipe.

Year	Authors/Source	Characteristics
2001	A. Gupta, J. Lee, and R. J. Koshel / AO	Analysis
2004	J. F. Van Derlofske and T. A. Hough / OE	Flux analysis
2004	L. R. Daveport, A. Hough and J. Cassarly / Proc. of SPIE	Efficiency
2005	S. –C. Chu and J. –L. Chern / OL	Analysis
2005	R. J. Koshel and A. Gupta / Proc. of SPIE	Efficiency
2006	Y. –K. Cheng and J. –L. Chern / JOSA	Analysis

In general, light pipe is an optical component that transferring the light from the input port to the output port, while the light pipe either carries the information or not. The light pipes used in FSC LCD backlight, except for guiding and illuminating the

light from the light source, still have some additional criterions. Therefore, it is necessary to know about some fundamental concepts of FSC LCD and what characteristic of light pipe should have in this display backlight system. Through the above consideration, the aim in this paper is as plain as a pikestaff.

1.1 Field-Sequential-Color Liquid Crystal Display (FSC LCD)

Color representation on conventional LCD has been accomplished with a combination of LC cells, micro color filters (CFs), and a white Cold Cathode Fluorescent Lamps (CCFL) backlight. However, only one third of the light from backlight can pass through the CFs, the other two-thirds energy is lost in this system. In addition, the color gamma is lower than National Television System Committee (NTSC) standard owing to the spectrum characteristic of the CCFL and CFs. [Fig. 1.2] Furthermore, the white backlight is always turned on and the blurring is an inherent character in this hold-mode display. These drawbacks prompt numerous researchers to improve performances of the conventional LCD in light-usage efficiency and image quality such as color saturation, contrast and viewing angle. [11]

Recently, the fast-response LCD, i.e. the Optically Compensated Bend (OCB) cell, has been developed. A nematic LC device, can readily be driven to exhibit combined on and off response time less than 10ms, and a high efficiency LED, the next generation light source, having the superiorities in the spectrum that could have a very narrow distribution resulting in a very wide color gamut when assembled as a backlight unit, and in its response time (on and off). [Fig. 1.2] Therefore, it is possible to introduce the FSC displaying method in LCD.

The FSC LCD temporally presents color on each pixel with red, green, and blue. The backlight illuminates the corresponded section simultaneously with the scanning of thin-film-transistor (TFT). Spatial refresh is performed by scanning from top to

bottom, that taking on the entire duration of one refresh frame.

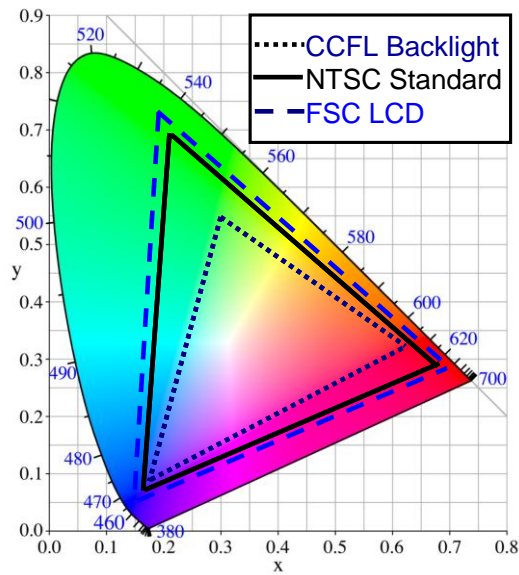


[Fig. 1.2] CIE color space diagram

For example, the backlight was determined to be equipped with 10 light pipes while the following condition should be satisfied.

$$[1 \text{ field time}] \geq [\text{scanning time of the whole gate lines}] / [\text{pipe number}] + [\text{response time of liquid crystal}] + [\text{backlight flashing time}]$$

One color field has duration of 1/180 sec (5.6 msec). The OCB-mode LC used in the prototype has a response time of a couple of milliseconds at gray-level transitions. The duty cycle of the illumination pulse is limited to about 50%. For a 7-in backlight, assuming the total number of gate lines is 600. If a light guide is divided into ten light pipes, a single linear light pipe of the backlight will be in charge of 60 lines of the TFT pixel array correspondingly, and the scanning duration over those lines is about 0.5 msec, which is the acceptable tolerance for the LC response time. [Fig. 1.3] shows the simple time relation on scans of LC TFT-array cell and LED backlight.

This temporal impulse-driving method in combination with spatial scanning not only for lowering power consumption but also reducing the image blurs. However, the spatial-temporal scanning backlight still has certain issues such as light leakage and

the directivity of extraction light, which affect the display of the image. Accordingly, it is necessary to provide a collimating lighting system which can make it possible to obtain a narrow angular distribution and effectively reduce the light leakage between two adjacent light pipes. [12][13]

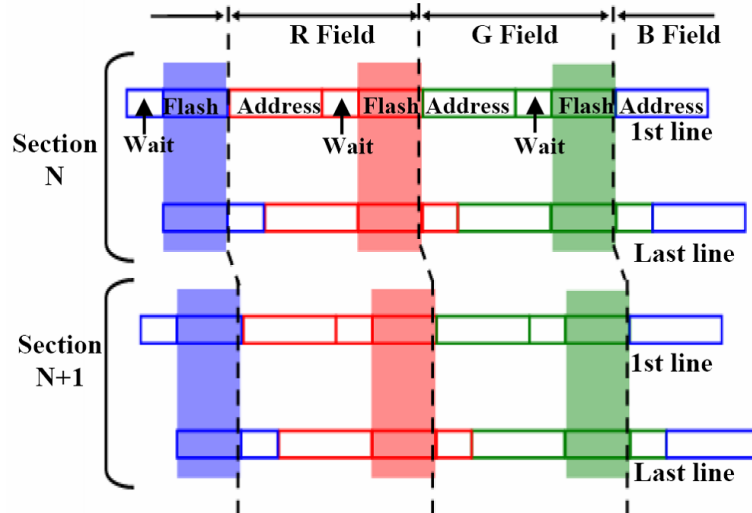
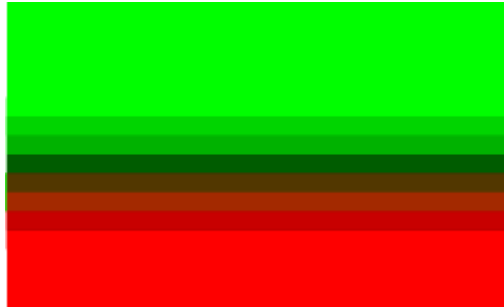


[Fig. 1.3] Timing chart for multi-flashing method

1.2 Scanning Backlights Application to FSC LCD

For the scanning backlights applied to FSC LCD, there are some particular concerns and constraints should be noticed. Considering the case of [Fig. 1.4(a)], because the red light from the LEDs will affect the adjacent region where the corresponded LEDs are turned off or another color LEDs are turned on at certain duration, the backlight should be partitioned into several divisions or blocks which are like light pipes. Each light pipe is isolated so that the LEDs illuminate only the corresponding field subject to the LC cell. [Fig. 1.4(b)] In addition, each interval between any two light pipes should not be observed from any viewing angle. Since the brighter or darker luminance of the shade somewhat has the influence on the appearance of the display. This requirement means that the certain proportion of light should leak into the interval or adjacent light pipes in order to eliminate the partition shade. [12]



(a)



(b)

[Fig. 1.4] The results of color image (a) Light guide without partition. (b) Light guide partitioned into linear light pipes.

[Table 1.2] Requirements for the backlight unit

Requirements	Objects
Distribution of the outcoupled energy	uniform along the pipe
Leakage to one distant light pipe	well suppressed
Partition shade between two adjacent light pipes	cannot be visible
Direction of illumination	in the normal direction of the output surface
Shape of the illumination	symmetric around the normal axis of the output surface
Light efficiency	to maximum

1.3 Motivation and Objective of this Thesis

The purpose of this thesis is to study and analyze the concept for the illumination light pipes applied to FSC LCD backlight. The light pipes using refractive or reflective micro structures as outcouplers to control the light output direction and distribution. Actually, reflective micro structures have the better controlling of the direction of illumination than the refractive micro structures. For convenience, the objectives that we want to achieve can be identified as [Table 1.2]. The proposed prototype consists of LED light sources, collimating light bars, and linear light pipes. This collimating lighting system made it possible to obtain a narrow angular light distribution, and effectively diminished the occurrence of color dependence in the scanning backlight for FSC applications.

1.4 Organization of this Thesis

This thesis is organized as following: previous work and principle of illumination light pipes in Chapter 2. In Chapter 3, the simulations of some related paper design and our modal are presented. The experimental results and discussion are described in Chapter 4. Finally, the summary of this thesis and future works will be presented in Chapter 5.

Chapter 2

Principle of Illumination Light Pipe

2.1 Vector Form of ray-tracing equation [14]

2.1.1 Refraction Law

Snell's law defines the appearance of refraction in the plane of incidence [Fig. 2.1]

$$n \sin \alpha = n' \sin \alpha' \quad (2.1)$$

where n and n' are the indices of refraction of the respective materials, α and α' are the angle of incidence and the new angle of propagation respectively.

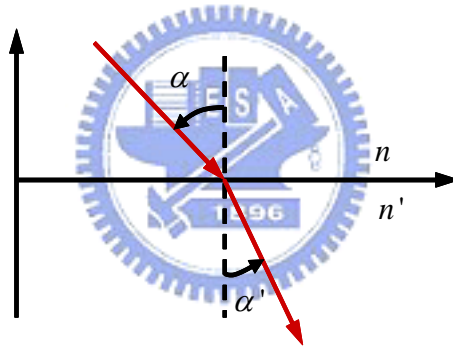


[Fig. 2.1] Representation of Snell's law in the plane of incidence

Snell's Law can be derived in the 3D space with the help of [Fig. 2.2].

Vector \vec{S} represents the incident ray with the magnitude n , and vector \vec{S}' represents the refracted ray with the magnitude n' . Therefore, the equation (2.1) may be rewritten as

$$|\vec{S}| \sin \alpha = |\vec{S}'| \sin \alpha' \quad (2.2)$$

The relationship between the incident refraction vector \vec{S}' and the incident vector \vec{S} is given by

$$\vec{S}' = \vec{S} - \vec{A} \quad (2.2)$$

where \vec{A} is the vector normal to the refractive surface with the unity vector \vec{r} . The magnitude of \vec{A} can be derived by

$$\begin{aligned}
|\vec{A}| &= \Gamma \\
&= |\vec{S}'| \cos \alpha' - |\vec{S}| \cos \alpha \\
&= n' \cos \alpha' - n \cos \alpha \\
&= n' \left[\left(\frac{n}{n'} \cos \alpha \right)^2 - \left(\frac{n}{n'} + 1 \right)^{1/2} \right] - n \cos \alpha \\
&= n' \left[\left(\frac{n}{n'} \frac{\vec{S} \cdot \vec{r}}{|\vec{S}| |\vec{r}|} \right)^2 - \left(\frac{n}{n'} + 1 \right)^{1/2} \right] - n \frac{\vec{S} \cdot \vec{r}}{|\vec{S}| |\vec{r}|} \tag{2.3}
\end{aligned}$$

The vectorial form of refraction is given by

$$\vec{S}' = \vec{S} + \Gamma \vec{r} \tag{2.4}$$

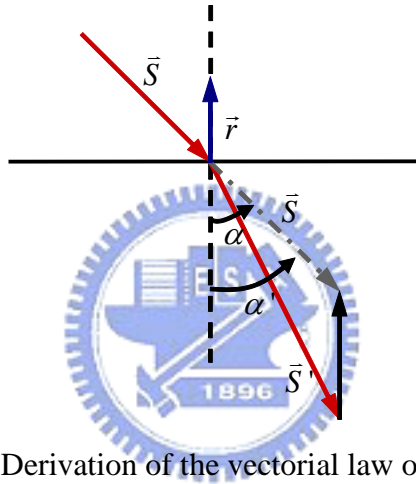


[Fig. 2.2] Derivation of the vectorial law of refraction

2.1.2 Reflection Law

In the plane of incidence, the deviation of optical rays due to reflection is defined by

$$\sin \alpha = -\sin \alpha' \tag{2.5}$$

where α and α' are the angle of incidence and reflected ray, respectively. From the above equation, it can be concluded that

$$\alpha = -\alpha' \tag{2.6}$$

The reflection law can be derived in the 3D space with the help of [Fig. 2.3].

Vector \vec{S} represents the incident ray and vector \vec{S}' represents the reflected ray.

Therefore, the equation (2.1) may be rewritten as

$$\vec{S}' = \vec{S} - 2\vec{A} \quad (2.7)$$

where \vec{A} is the vector normal to the reflective surface with the unity vector \vec{r} . The magnitude of \vec{A} can be derived by

$$|\vec{A}| = \vec{S} \cdot \vec{r} \quad (2.8)$$

The vectorial form of reflection is given by

$$\vec{S}' = \vec{S} - 2(\vec{S} \cdot \vec{r}) \vec{r} \quad (2.7)$$

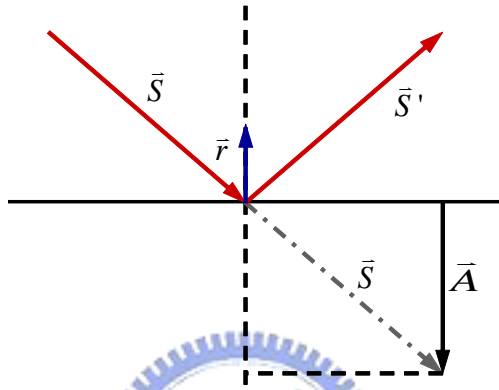


[Fig. 2.3] Derivation of the vectorial law of reflection

2.2 Fresnel Reflection

2.2.1 Reflection Coefficients

For the P (parallel to the plane of incidence) and S (perpendicular to the plane of incidence) polarization waves, the amplitude reflection coefficients are given by

$$r_p = \frac{n_1 \cos \alpha_2 - n_2 \cos \alpha_1}{n_1 \cos \alpha_2 + n_2 \cos \alpha_1} \quad (2.8)$$

$$r_s = \frac{n_1 \cos \alpha_1 - n_2 \cos \alpha_2}{n_1 \cos \alpha_1 + n_2 \cos \alpha_2} \quad (2.9)$$

where n_1 and n_2 are the indices of refraction of the respective materials, α_1 and α_2 are the angle of incidence and the angle of propagation respectively.

The reflectance and transmittance for polarized light are defined as

$$R_p = r_p^2 \quad (2.10)$$

$$R_s = r_s^2 \quad (2.11)$$

$$T_p = 1 - R_p \quad (2.12)$$

$$T_s = 1 - R_s \quad (2.13)$$

When the light is unpolarized, the reflectance R and transmittance T are defined as the average of the polarized case

$$R = \frac{R_p + R_s}{2} \quad (2.14)$$

$$T = \frac{T_p + T_s}{2} \quad (2.15)$$

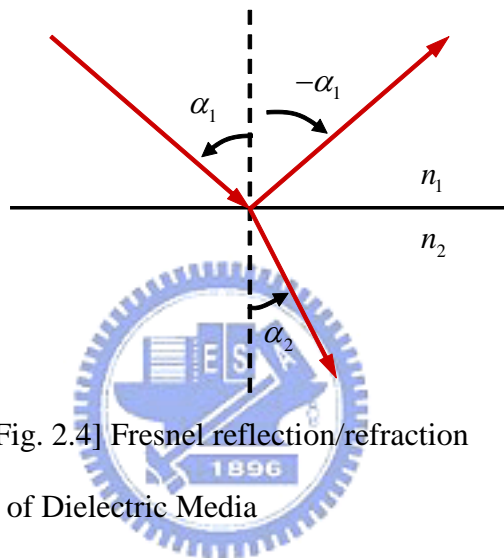


[Fig. 2.4] Fresnel reflection/refraction

2.2.2 Typical Reflectance of Dielectric Media

In multiple reflections case, it should be considered that the Fresnel reflection has essential influence on total efficiency of the illumination light pipes. The transmittance and reflectance curves of polarized and unpolarized light for dielectric materials under this two conditions (1) $n_1 = 1.0$, $n_2 = 1.5$ (2) $n_1 = 1.5$, $n_2 = 1.0$ are shown in [Fig. 2.5] and [Fig. 2.6], respectively.

there is a critical angle α_c for the case in [Fig. 2.6]. When the angle of incidence is greater than α_c , light is loss less reflected by total internal reflection (TIR). The critical angle is given by

$$\alpha_c = \sin^{-1}\left(\frac{n_2}{n_1}\right) \quad (2.16)$$

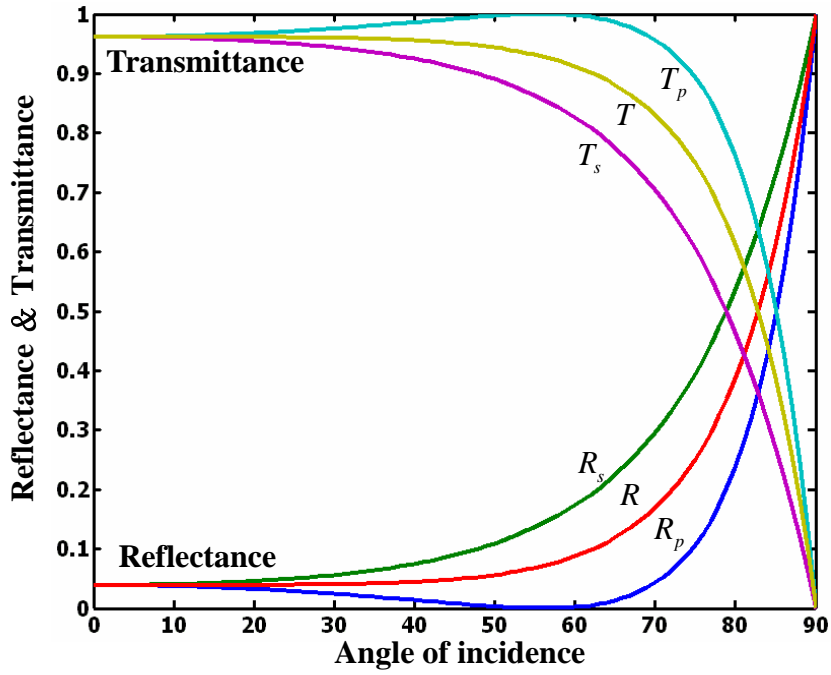


[Fig. 2.5] Transmittance and Reflectance for $n_1 = 1.0$, and $n_2 = 1.5$.

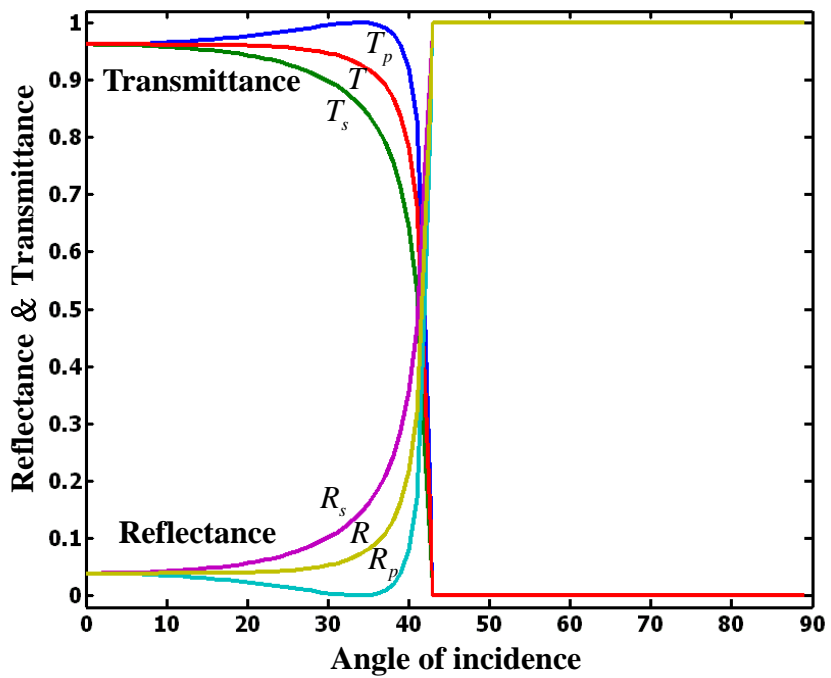
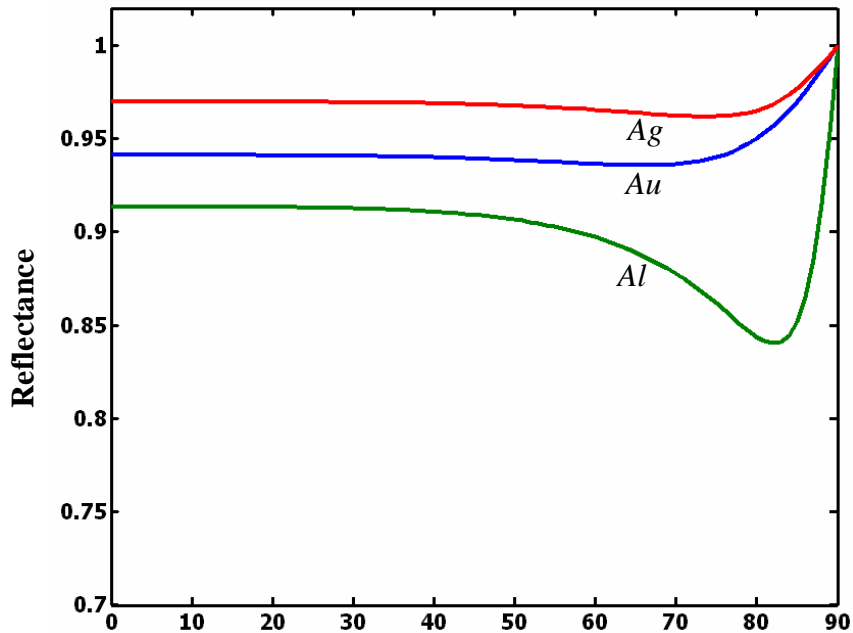


[Fig. 2.6] Transmittance and Reflectance for $n_1 = 1.5$, and $n_2 = 1.0$.

2.2.3 Typical Reflectance of Metal

In general, when the light pipe is coated by a certain metal, we should take into account the light that is absorbed by the material. It can be critical losses while the light is guided by multiple metallic reflections. The reflectance curves of unpolarized

light for gold (Au), aluminum (Al), and silver (Ag) under this two conditions (1) $n_1 = 1.0$ (2) $n_1 = 1.5$ are shown in [Fig. 2.7] and [Fig. 2.8]. At the wavelength of 652nm, the complex refractive indices of these material are $n_{Au} = 0.166 + 3.15i$,



$n_{Al} = 1.39 + 7.65i$, and $n_{Ag} = 0.140 + 4.15i$.

[Fig. 2.7] Reflectance of Au, Al, and Ag for $n_1 = 1.0$

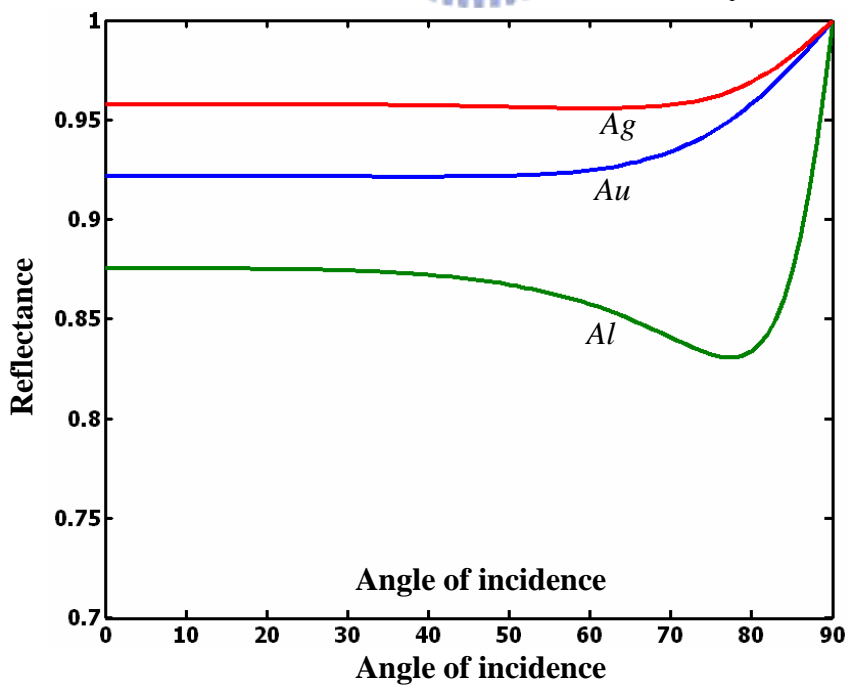


[Fig. 2.8] Reflectance of Au, Al, and Ag for $n_1 = 1.5$

2.2.4 Reflectance of the Pipe-Air-Metal Interface

Considering the illumination light pipe surrounded by a reflector, the lost light might be redirected to the desired direction and the proportion of reflected light can be calculated. The diagram is depicted in [Fig. 2.9]. At wavelength of $652nm$, The refraction indices of Al reflector and light pipe are $n_{Al} = 1.39 + 7.65i$ and $n_1 = 1.5$ correspondingly. Assuming the calculated parameters are as follows: the angle of incidence α_1 , the angle of refraction α_2 , and several reflectance and transmittances. The total reflected energy is the sum of contribution of each inter-reflection R_i .

$$\begin{aligned}
 i=0: \quad R_0 &= R_{12}(\alpha_1) \\
 i=1: \quad R_1 &= T_{12}(\alpha_1) \cdot R_{23}(\alpha_2) \cdot T_{21}(\alpha_2) \\
 i=2: \quad R_2 &= T_{12}(\alpha_1) \cdot R_{23}(\alpha_2) \cdot R_{21}(\alpha_2) \cdot R_{23}(\alpha_2) \cdot T_{21}(\alpha_2) \\
 i=3: \quad R_3 &= T_{12}(\alpha_1) \cdot R_{23}(\alpha_2) \cdot R_{21}(\alpha_2)^2 \cdot R_{23}(\alpha_2)^2 \cdot T_{21}(\alpha_2) \quad (2.17)
 \end{aligned}$$

The total reflected energy is defined as

$$\begin{aligned}
 R_{tot} &= \sum_i R_i \\
 &= R_{12}(\alpha_1) + T_{12}(\alpha_1) \cdot R_{23}(\alpha_2) \cdot T_{21}(\alpha_2) \cdot [1 + R_{21}(\alpha_2) \cdot R_{23}(\alpha_2) + R_{21}(\alpha_2)^2 \cdot R_{23}(\alpha_2)^2 + \dots] \\
 &= R_{12}(\alpha_1) + \frac{T_{12}(\alpha_1) \cdot R_{23}(\alpha_2) \cdot T_{21}(\alpha_2)}{1 - R_{21}(\alpha_2) \cdot R_{23}(\alpha_2)} \quad (2.18)
 \end{aligned}$$

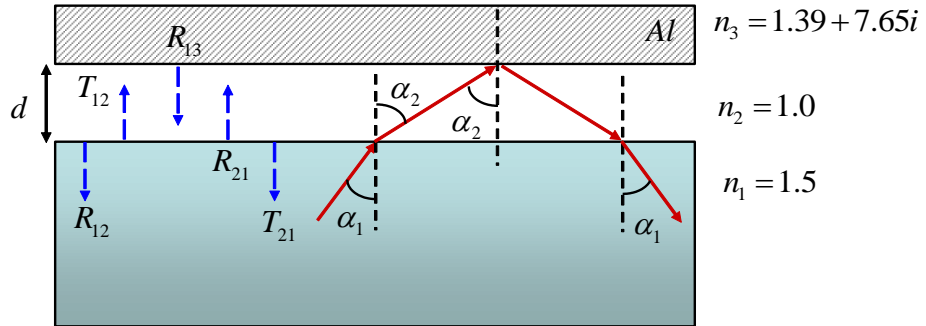


[Fig. 2.9] Parameters of the pipe-reflector configuration

The relation between the reflected energy and the angle of incidence is shown in [Fig.

2.10]. Undoubtedly, when $\alpha_1 > \alpha_c$, there has TIR phenomenon.

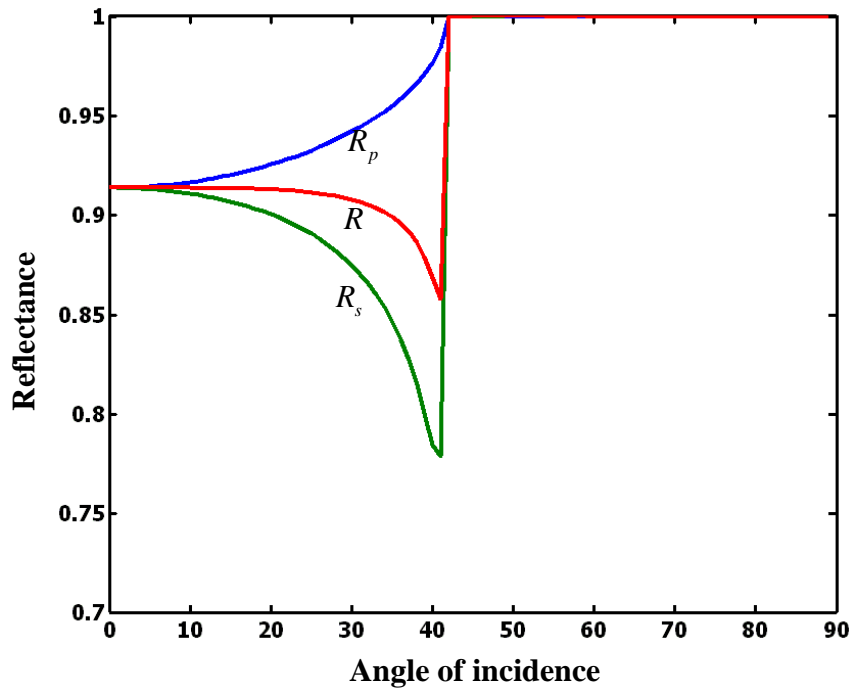


[Fig. 2.10] Reflectance of the pipe surrounded by an Al reflector

From the [Fig. 2.9] and equation (2.18), the absorbed energy or the angle of ray reaching the reflector do not affected by the air gap d , but the air gap d should be larger than the penetration depth δ of the evanescent light to avoid any losses by tunneling effect. The penetration depth is given by

$$\delta = \frac{\lambda}{2\pi\sqrt{n_1^2 \sin^2 \alpha_1 - n_2^2}} \quad (2.19)$$

2.3 Radiometry and Photometry Quantities

2.3.1 Radiometry

Radiometry is the science of measuring light in any portion of the electromagnetic spectrum. In practice, the term is usually limited to the measurement of infrared, visible, and ultraviolet light using optical instruments. The fundamental radiometric quantities are shown in [Table 2.1].

[Table 2.1] Energy-based Units

Quantity	Symbol	Definition	Typical Units
Radiant Energy	Q		joule
Radiant Energy Density	u	dQ/dV	joule/m ³
Radiant Flux (Power)	$\Phi(P)$	dQ/dt	watt
Radiant Exitance	M	$d\Phi/dA$	watt/m ²
Irradiance	E	$d\Phi/dA$	watt/m ²
Radiance	L	$d^2\Phi/dAd\Omega$	watt/m ² (/sr)
Radiant Intensity	I	$d\Phi/dAd\Omega$	watt/sr

From this table, there are some key points should be emphasized

- ◆ Q is the radiant energy of a collection of photons (as in a laser pulse); the energy of a single of a single photon is $h\nu$.
- ◆ M pertains to radiation leaving a surface; E pertains to radiation incident on a surface.
- ◆ dA_{\perp} is the area element, dA , projected onto a plane \perp to the light of sight [Fig. 2.11]

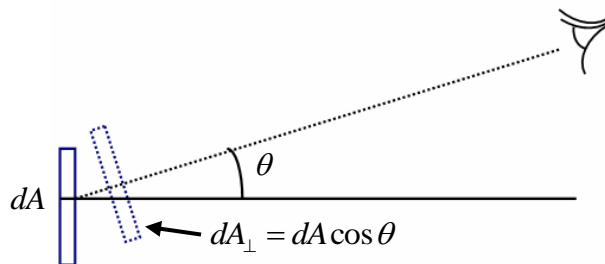
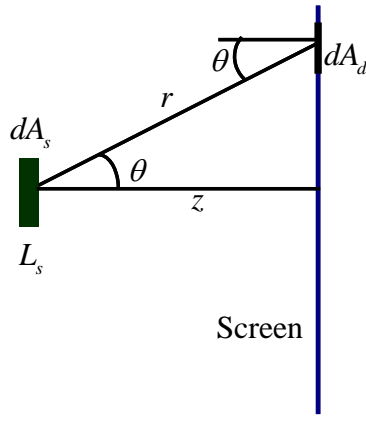


[Fig. 2.11] schematic diagram of projection area

For example, there is a small extended lambertian source with the area dA_s and source radiance L_s (L_s is independent of direction.). The irradiance dE_d of the detected area dA_d on the illumination screen is derived from



$$d^2\Phi_d = \left(\frac{d^2\Phi_s}{dA_{s,\perp}d\Omega_s}\right)dA_{s,\perp}d\Omega_s$$

$$d^2\Phi_d = L_s dA_{s,\perp} \left(\frac{dA_{d,\perp}}{r^2}\right)$$

$$d^2\Phi_d = \frac{L_s dA_s \cos\theta dA_d \cos\theta}{(z/\cos\theta)^2}$$

$$d^2E_d = \frac{L_s dA_s \cos^4\theta}{z^2} \quad (2.20)$$

[Fig. 2.12] Simple radiometry problem

as shown in [Fig. 2.12], where z is the normal distance from source to screen, and r is equal to $z/\cos\theta$. The equation (2.20) shows the $\cos^4\theta$ law, which is conventionally stated: For a small extended source, the irradiance on a flat surface is direct proportional to quartics of $\cos\theta$. In the above discussion, no mention has been made of the spectral characteristics of the radiation. However, every source has its own radiation spectral distribution. The spectral radiometric quantities can be obtained by differentiating any of the Energy-based units with respect to spectral quantity (λ, ν , or $h\nu$).

2.3.2 Photometry

Photometry is the science of measuring visible light in units that are weighted according to the sensitivity of the human eye. It is a quantitative science based on a statistical model of the human visual response to radiation -- that is, our perception of light -- under carefully controlled conditions. The basic photometric unit of radiant power is lumen, which is defined as a luminous flux emitted into a solid of one steradian by a point source whose intensity is 1/60 of that of 1 cm^2 of a blackbody at the solidification temperature of platinum (2042 K). From the lumen definition, it can be determined that one watt of radiant energy at the wavelength of maximum visual sensitivity ($0.555\ \mu\text{m}$) is equal to 680 lumens. Therefore, the luminous flux emitted by a source with a radiant flux $\Phi_\lambda(\lambda)$ is given by

$$\Phi_v = 680 \int V_\lambda(\lambda) \Phi_\lambda(\lambda) d\lambda \quad (2.21)$$

where the $V_\lambda(\lambda)$ is the visual response function which is depicted in [Fig. 2.13].

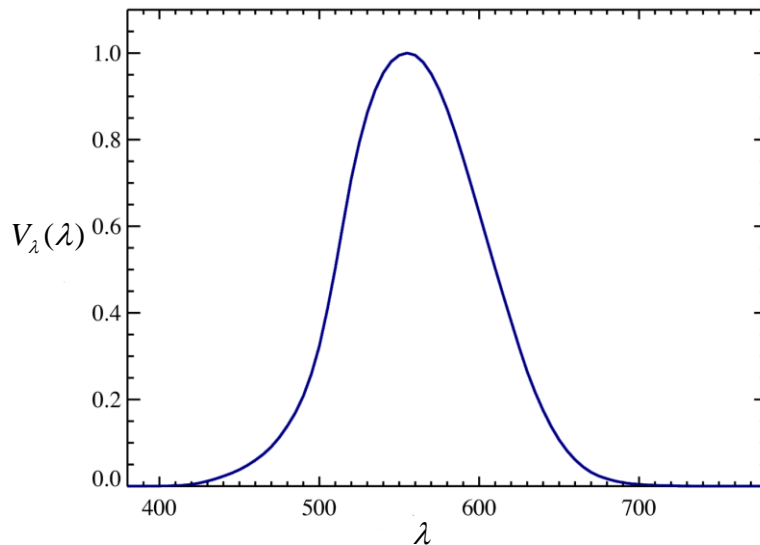


[Fig. 2.13] Human visual response function

The terminology of photometry has grown through engineering usage, and is thus far from orderly. Special terms have derived from special usages, and many such terms have survived. A tabulation of photometric units is given in [Table 2.2].

[Table 2.2] Photometric Quantities

Quantity	Symbol	Definition	Typical Units
Luminous Energy	Q_v		$\text{lm} \cdot \text{s} = \text{talbot}$
Luminous Density	u_v	dQ_v/dV	$\text{lm} \cdot \text{s}/\text{m}^3$
Luminous Flux	Φ_v	dQ_v/dt	lumen (lm)
Luminous Exitance	M_v	$d\Phi_v/dA$	$\text{lm}/\text{m}^2 = \text{lux (lx)}$
Illuminance	E_v	$d\Phi_v/dA$	lx
Luminance (Brightness)	L_v	$d\Phi_v/dAd\Omega$	$\text{lm}/\text{m}^2/\text{sr} = \text{nit(nt)}$, $\text{lm}/\text{ft}^2 = \text{footcandle}$
Luminous Intensity	I_v	$d\Phi_v/d\Omega$	$\text{lm}/\text{m}/\text{sr} = \text{candela(cd)}$

2.4 The Light Pipe Concept

The light pipe's function consists in transforming a quasi-point light source such as LED into an extended surface light source. When light is guided inside the pipe with total internal reflection (TIR), it may encounter the outcoupling zones

which are arranged at the pipe surface so that a part of light is extracted out from the pipe. The outcoupled lighting distribution can be controlled by choosing the size and shape of the pipe and the spatial distribution of the outcouplers along the pipe. The configurations of the pipes could be the linear light pipe, the circular light pipe, or the plate light pipe, depending on the required optical function. [Fig. 2.14]

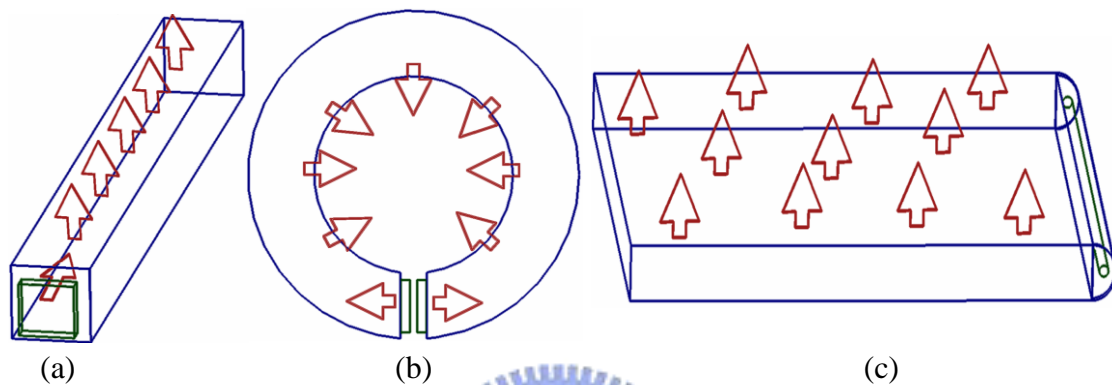


[Fig. 2.14] (a) Linear light pipe. (b) Circular light pipe. (c) Plate light pipe.

The next sections discuss and describe the influences of the shape of the pipe cross section and the type of outcouplers on the angular spectrum and the lighting distribution of illumination rays.

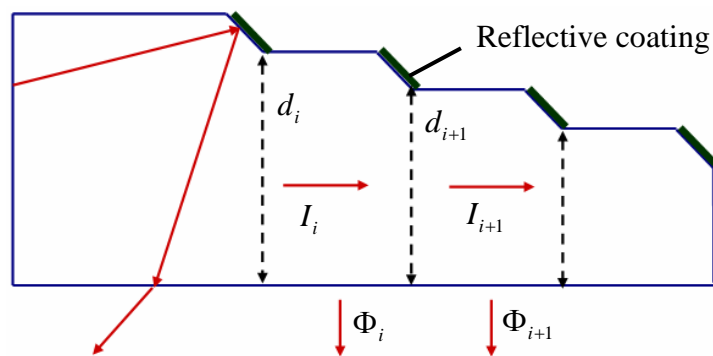


[Fig. 2.15] Discontinuous variable cross-section light pipe

2.4.1 Variable Cross Section Light Pipe

The variation of the cross section can simply be classified into continuous or discontinuous cross-section light pipe. For the discontinuous case shown in [Fig. 2.15], the amount of I_{i+1} flux coupled out from the $I + I^{th}$ section of the pipe is given

as

$$I_{i+1} = \frac{d_{i+1}}{d_i} I_i \quad (2.22)$$

where I_i is the guided flux at the i^{th} section of the pipe, and d_i and d_{i+1} are the sizes of the respective cross-sections. The locally outcoupled flux is then defined as

$$I_i - I_{i+1} = I_i \left(1 - \frac{d_{i+1}}{d_i}\right) \quad (2.23)$$

On the other side, the propagation angle α_i of the guided rays in continuous type such as the wedge light pipe is changed at each intersection with the oblique face. When the propagation angle is smaller than the critical angle α_c , the guided rays that do not obey the total internal reflection law will be extracted out. As shown in the [Fig. 2.16], assuming the A line represents the ideal reflection surface, B line and C line represent the equivalent output surface of the light pipe and the ray for different illuminated angle correspondingly. The general equations for the B and C line are derived as

$$\begin{aligned} B : y &= [\tan(2\alpha_s \cdot i)]x \\ C : y_0 - y &= (x - x_0) \tan \alpha \end{aligned} \quad (2.24)$$

where the lambertian light source located at the position (x_0, y_0) , and α_s and α are the slope angle of the pipe surface and the angle of ray incident into the light pipe respectively. From the equation (2.24), the x, y values can be given as

$$\begin{aligned} x &= \frac{y_0 + x_0 \tan \alpha}{\tan \alpha + [\tan(2\alpha_s \cdot i)]} \\ y &= y_0 - (x - x_0) \tan \alpha \end{aligned} \quad (2.25)$$

for a specific angle α , there will have a corresponding number i . Therefore, the equivalent light output position x' is calculated by

$$x' = \sqrt{x^2 + y^2} \quad (2.26)$$

x' is the actual location of the x axis. The analysis for the rays illuminate to the upper half region is the same as the above consideration.

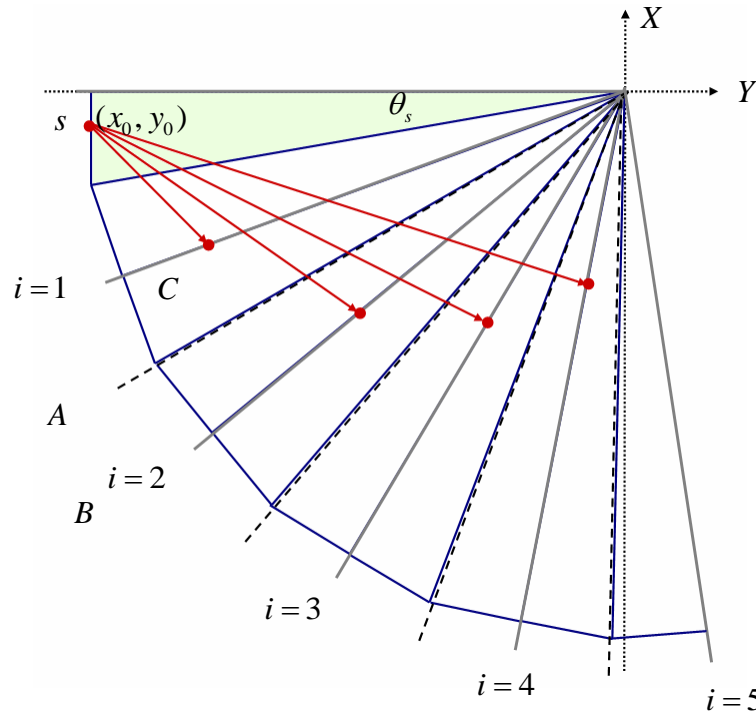


[Fig. 2.16] The equivalent modal for the light propagate in the wedge light pipe

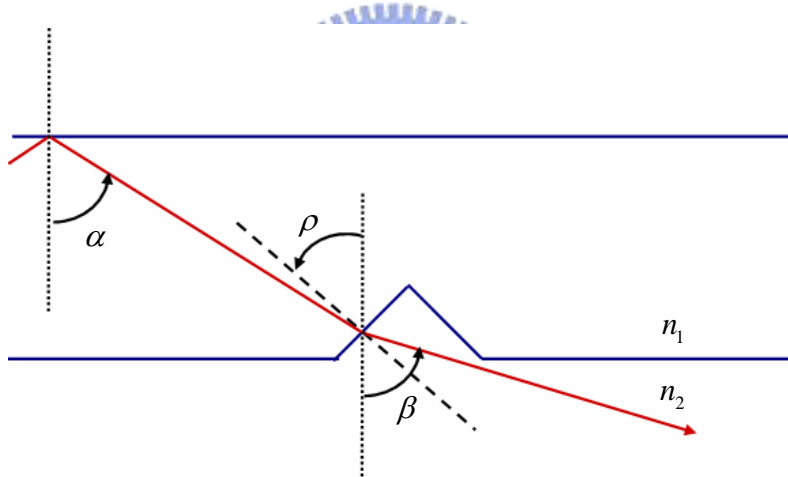


[Fig. 2.17] Example of refractive outcoupling case.

2.4.2 Refractive and Reflective Outcouplers

The objective that the refractive or reflective outcouplers are discontinuously arranged along the pipe surface is to redirect and redistribute the propagated light into illumination light partially. For the refractive case, as shown in [Fig. 2.17], the outcoupling angle β is calculated from the Snell's law as

$$\beta = \sin^{-1}\left[\frac{n_2}{n_1} \sin(\alpha - \rho)\right] + \rho \quad (2.27)$$

where α is the incident angle, ρ is the inclination of the refractive surface, n_1 is the

refractive index of the media surrounding the pipe, and n_2 is the refractive index of the pipe. The equation (2.27) reveals the outcoupling angle β is the function of inclination of the refractive surface ρ and the incident angle α . [Fig. 2.18] shows the relation among these parameters. In this figure, the material of the pipe is pmma ($n_2 = 1.49$) and the environment is air ($n_1 = 1.0$). The angle of incident α from 47.8° to 90° which can propagate inside the light pipe corresponding to the gray region. It is quite obvious that most of the outcoupled rays depart from the pipe at the large angles. This is not practical for illumination requirement which usually want to illuminate normal

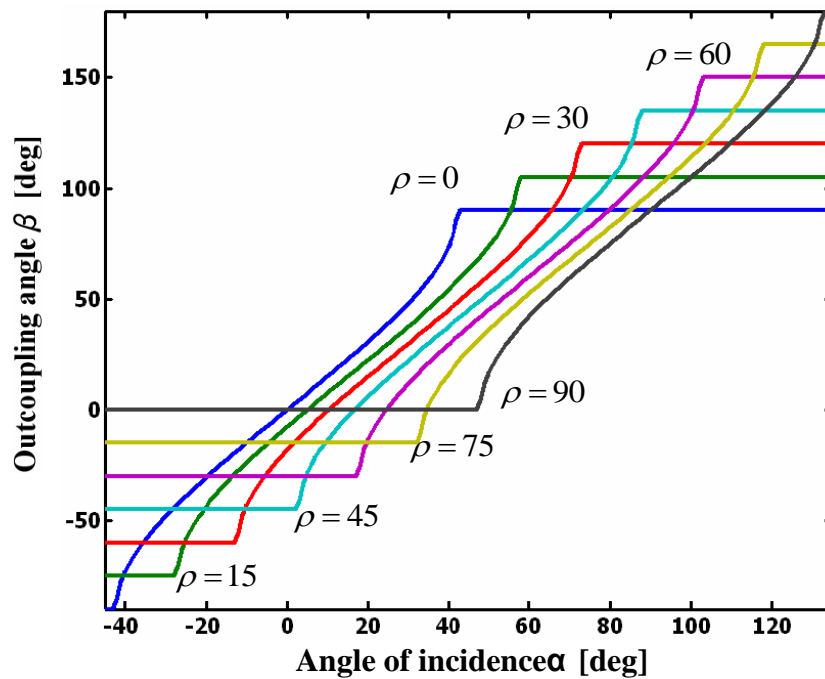


[Fig. 2.18] Outcoupling angles achieved by refraction for different orientations

As for the refractive case, the reflective outcouplers are also discontinuously arranged along the pipe surface which deviate the direction of the guided rays and then turn into illuminated rays. As illustrated in [Fig. 2.19], the reflective micro prism can be selectively coated micro-prisms or the TIR micro-prism. The relation between the outcoupling angle β , the prism orientation ρ , and the angle of the incident rays α is determined by

$$\beta = \sin^{-1}\left[\frac{n_2}{n_1} \sin(-\alpha + 2\rho)\right] \quad (2.28)$$

For the case where $n_1=1.0, n_2=1.49$ (pmma) in the graph of [Fig. 2.20], the gray region corresponds to the rays guided in the pipe by TIR. In this figure, for a given angle of incident α , any extracting direction β can be selected by choosing the right prism orientation ρ .

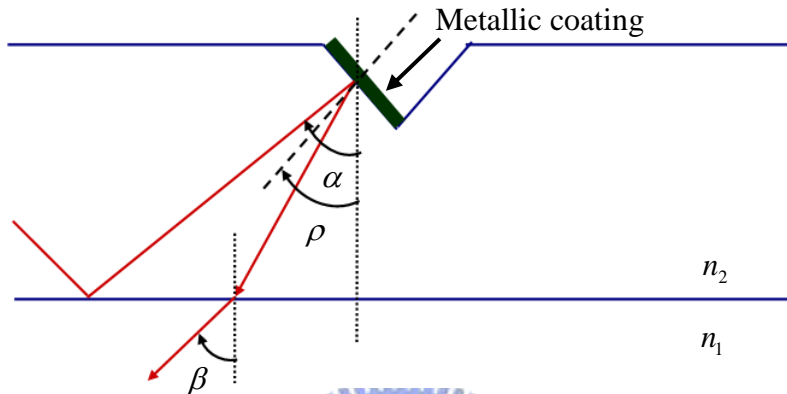


[Fig. 2.19] Outcoupling produced by a reflective micro-prism

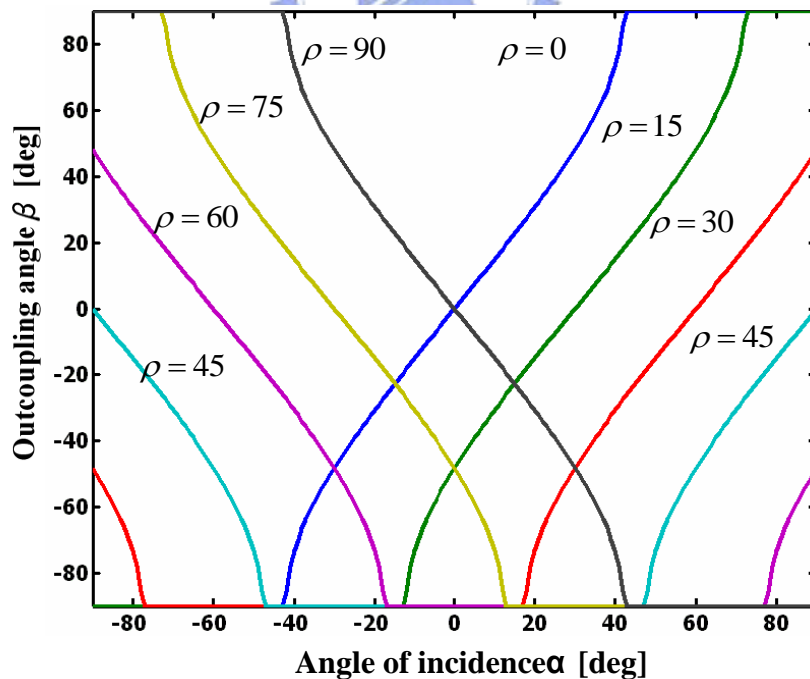


[Fig. 2.20] Outcoupling angles achieved by reflection for different orientations

Chapter 3

Simulations and Discussions

3.1 Introduction

Based on the principle in chapter 2, the simulation model for the light pipe applied to FSC LCD backlight was established. First of all, the component parts used in the simulated backlight should be clearly described and defined. Besides, we should notice that the different kind of out coupler will result in there own light distribution. Therefore, the briefly discussion for different kind of out coupler will be given. After that, our solution for this kind backlight light system was designed and optimized.

3.2 Simulation Tool

The optical simulation tool Tracepro™, developed by Lambda Research Corporation was used to optimize the FSC LCD backlight system and simulate its angular distribution as well as uniformity on output surface of the backlight.

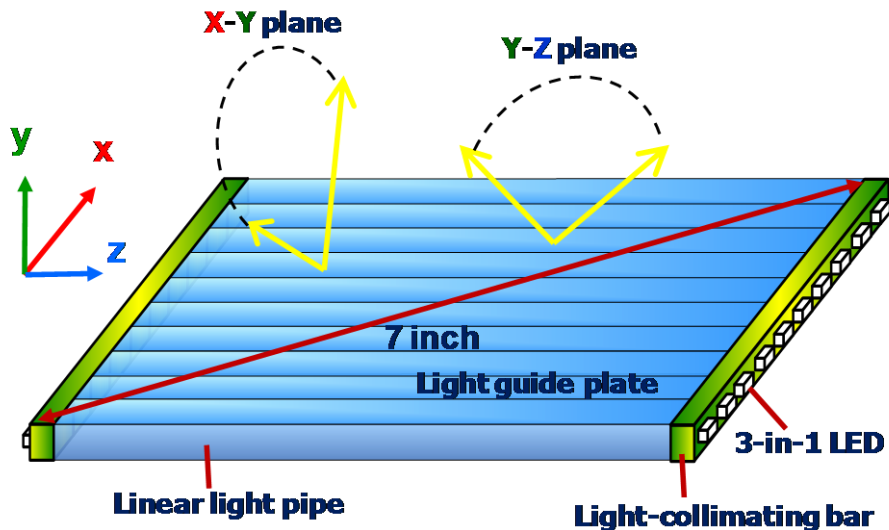


[Fig 3.1] Schematic diagram of the proposed backlight system

3.3 Simulation Modal of FSC LCD Backlight System

The prototype of the FSC LCD backlight system consists of three main parts as

shown in [Fig 3.1]:

1. 60 packages of 3-in-1 full color LEDs used as the light sources. The angular distribution of the LEDs was set for simulation as a lambertian illumination. The dominating wavelengths of $\lambda_R = 622nm$, $\lambda_G = 527nm$, and $\lambda_B = 470nm$ for the red, green, and blue chips was set correspondingly and the chromaticity of these three colors are $(x,y) = (0.7362, 0.2634)$, $(0.1656, 0.7406)$, $(0.1453, 0.0597)$, respectively, that resulting in a color gamut larger than 120% of the NTSC (National Television Standards Committee) standard.
2. Two light-collimating bars (120.5mm×2.5mm×3mm) were attached between LED light sources and the light guide plate to reduce the X-Z planar divergence of incident light. This enhances the coupling ratio from source to pipe. Besides, the light-collimating bar was expected to diminish the unevenness distribution of the light intensity near the light source. [Fig. 3.2]
3. Ten linear light pipes (12mm×160mm×3mm) with micro-groove structures over the bottom that control the direction of the light extraction on the Y-Z plane as well as the color uniformity along the pipe direction. The metallic coating Au on the bottom of the pipes was defined by its complex refractive index, which was wavelength dependent. The light leakage was controlled by the total internal reflection of the sidewalls of the light pipe. Consequently, each field could represent color without inter-field erroneous color mixture.

During the ray-tracing process, the detector was placed at the position where the analysis of the spatial and angular distribution of the illuminating light served for the evaluation of the design performance. For convenience, we made a table of the specification of the desired prototype FSC LCD, which is shown in [Table 3.1]

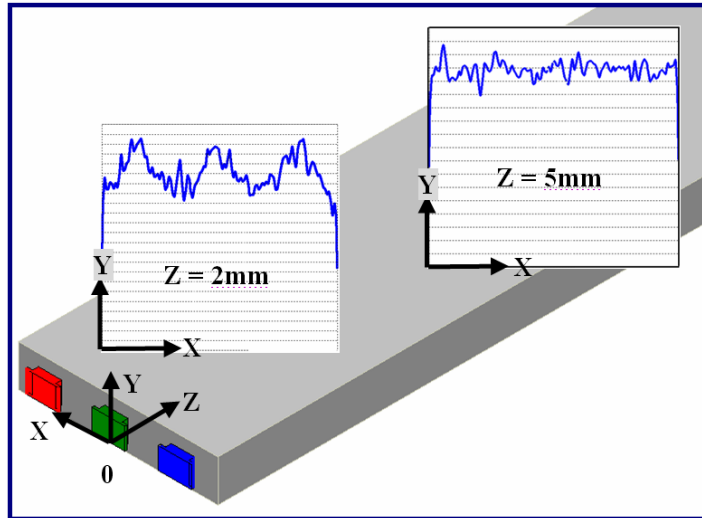


[Fig 3.2] The repartition of the flux at different positions inside the clear light pipe
 The refractive index of 1.49 for light pipes was set, which is the same as PMMA. It can be observed that there exists a non-uniformity of light distribution at the proximity to the source, i.e. $z = 2\text{mm}$. Afterward the distribution of the flux becomes uniform through $Z > 5\text{mm}$.

[Table 3.1] The specification of the proposed FSC LCD

Active area	7-inch diagonal Aspect ratio 4:3 800(H) × 600(V) pixels
Structure	<ol style="list-style-type: none"> 60 packages of 3-in-1 LEDs Two light-collimating bars Ten linear functional light pipes
Colors	Field sequential color method
Refresh	60 frames/sec, 180 fields/sec R, G, B fields
Objective	<ol style="list-style-type: none"> Suppressing the light leakage of less 10% The emergent light with half angle 30° The uniformity and efficiency reach to 80% and 70% respectively.

3.4 The Determination for the Type of the Micro Structure

In order to present the color correctly, the angular distribution of the out-coupled rays must be well controlled for the FSC LCD backlight. In other words, the light reflected by the out-coupler should have the character of high directivity and should be normal to the output surface. As discussed in chapter 2.4.2, the reflective out-coupler seems the better candidate than the refractive type. According to the reference, [12] it also shows that the micro groove is much suitable than the bump or hole-type micro-reflector owing to the micro-reflector will lead to the wider angular distribution as the result depicted in [Fig 3.3]. Recently, some literatures brought up advanced micro structures named double prisms, [15] to narrow the light distribution further with no brightness enhance film or diffuser. [Fig 3.4] However, considering the cost of production and the manufacture technology, the discrete arrangement of the micro groove structures fabricated by diamond turning was the elected method to be used.

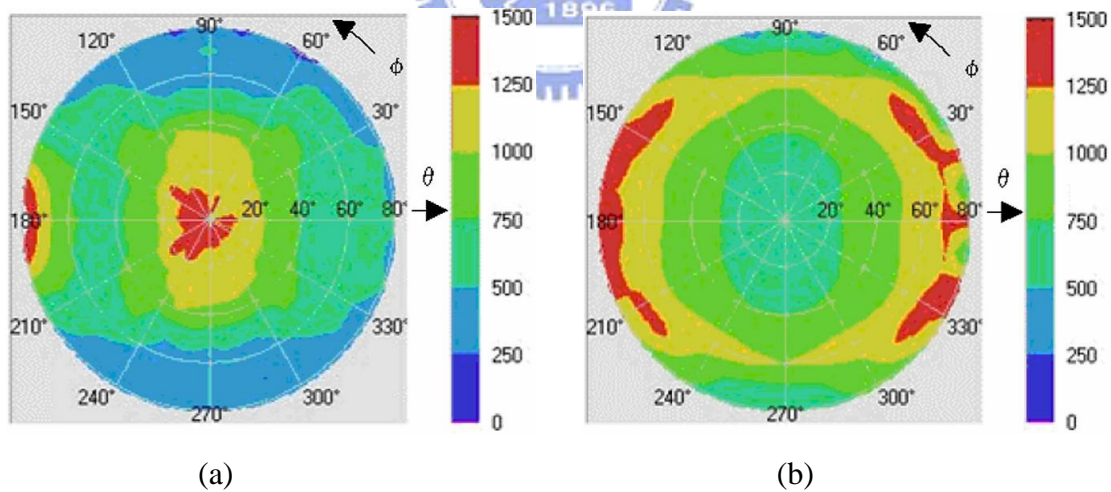


[Fig 3.3] (a) Angular light distribution measured on a bare linear light guide with uniformly positioned micro-prisms on the front and gradationally positioned micro-prisms on the rear. (b) Angular light distribution on a bare linear light guide with micro-reflector array on the rear.

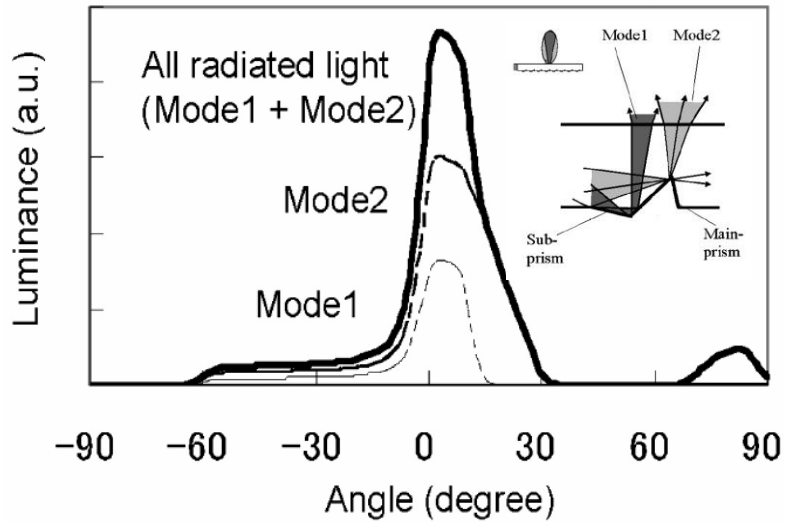


[Fig 3.4] The all radiated light from double prism (Mode1 is the radiated light from the sub prism and Mode2 is the radiated light from the main prism).

Besides, although the wedge-type light pipe has higher light efficiency than the linear light pipe, the direction of most illuminating rays deviates from the normal of the output surface. Those out-coupled rays leaved the pipe at grazing angle are not practical for most applications. Therefore, the external correction plate such as a TIR prism sheet should be combined with the pipe. [Fig. 3.5] [16]

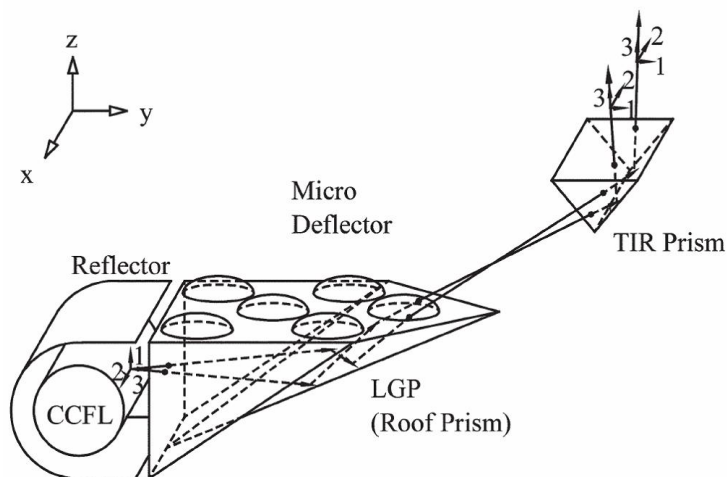


[Fig. 3.5] The wedge-type light pipe needs the TIR prism sheet to modify the illumination light.

3.5 Optimization of FSC LCD Backlight System

3.5.1 Optimization of the light-collimating bars

In this section, all of the work is done by my cooperator Cho-Chih Chen. As mentioned before, the light-collimating bar was used to reduce the X-Z plane divergence of the LED. To do such function, there are several different kinds of micro-structures were built on the out-coupling side of the bar and they can be classified into three types of zones, as shown in [Fig 3.6].

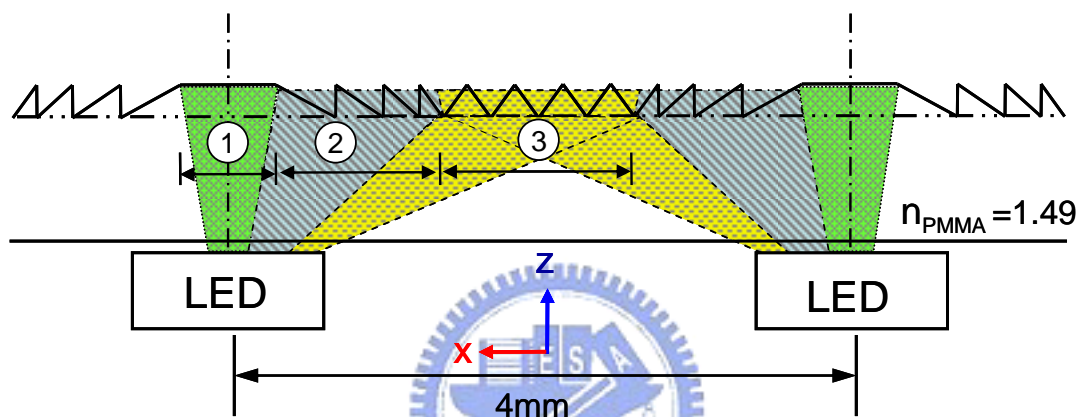


[Fig 3.6] The zones of light-collimating bar: ① The transmitting zone corresponded to the light source which had an incident angle approximately within $\pm 15^\circ$. ② The blaze zone where saw-toothed shapes were formed was defined as the area within the incident light with angles larger than 15° but smaller than about 30° . ③ The prism zone with isosceles triangular prism pattern was utilized to refract the light with angles larger than 30° . This zone was illuminated not only by the corresponding LED but also by adjacent LED.

The angular distribution of the extraction light from the light-collimating bar was shown in [Fig 3.7]. According to this result, the light-collimating bar remarkably reduced the X-Z plane divergence of the incident light.

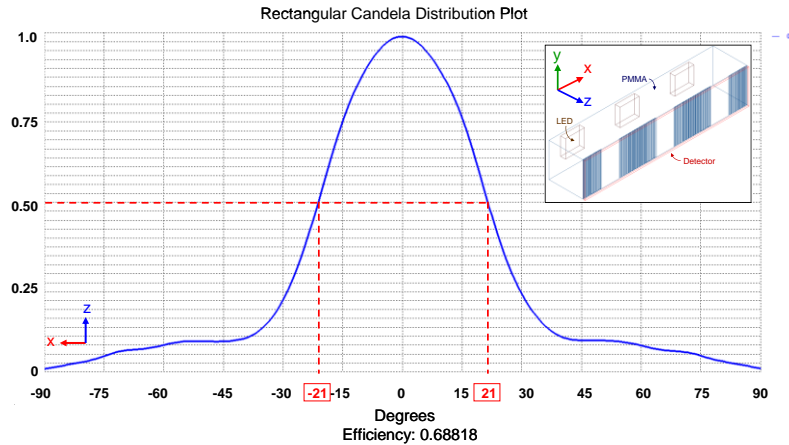


[Fig 3.7] The angular distribution of the extraction light from light-collimating bar.

3.5.2 Optimization of the linear light pipe

After establishing the modal of light-collimating bar, the distribution of the light from the bar's out-coupling surface had been obtained already and it can be treated as the new light source at this time for the following simulation. The related parameters of the micro grooves over the bottom of the linear light pipe should be clearly defined first. As shown in [Fig 3.8], the parameters of the groove structure include the orientation of the groove orientation ρ , groove pitch p , groove depth d , and groove width along the Z-axis w_z , along the X-axis w_x . In fact, the groove orientation affects the angular distribution of the illuminated rays while the groove width and pitch determine the illumination uniformity.

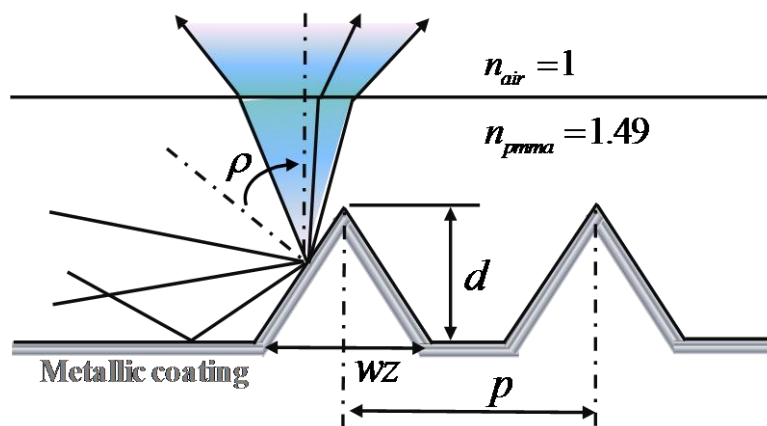


[Fig 3.8] The parameters of the micro-groove structure

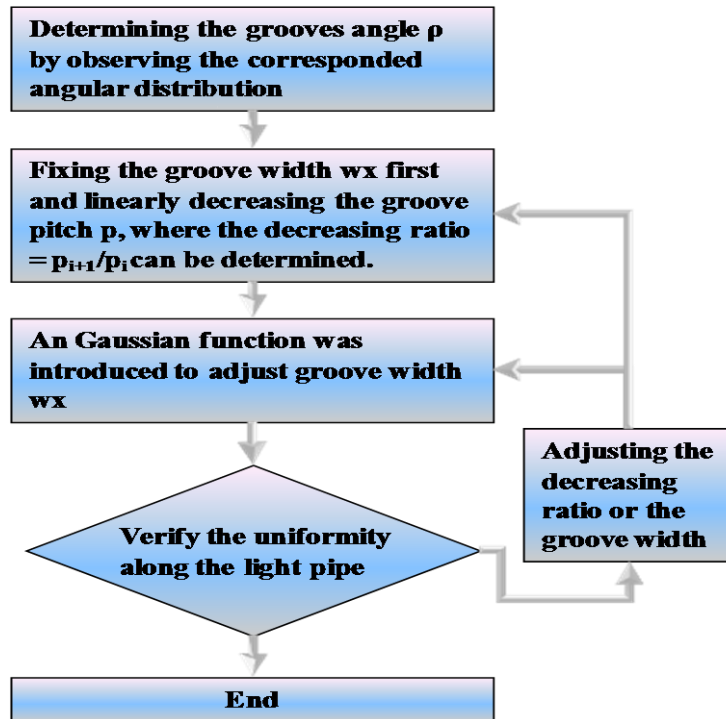


[Fig 3.9] The optimization flowchart

The optimization flowchart is depicted in [Fig 3.9]. First, the desired direction of the out-coupled rays could be modified by choosing a proper groove orientation. The simulation in this part was simply carried out under a uniform distribution of the micro grooves due to the grooves arrangement does not influence the directionality. From the discussion in chapter 2.4.2, the relation about the out-coupled angle β and the prism orientation ρ was depicted in [Fig 2.20] where the gray region corresponds to the rays guided in the pipe by TIR. The line represented the out-coupled angle $\beta = 0^\circ$ intersects to the curves of the prism orientation at $\rho = 30^\circ$ and $\rho = 45^\circ$. Accordingly, the angular distribution simulated under the various groove orientations between $\rho = 30^\circ$ and $\rho = 45^\circ$. The result was shown in [Fig 3.10]. The angular distribution at groove angle $\rho = 43^\circ$ had the narrowest divergent angle of about $\pm 30^\circ$ and symmetry to the normal of output surface compared with other angles. It implied that a tolerance of $\pm 2^\circ$ around the optimal groove orientation was acceptable and the requirement could be achieved by most of the fabrication process. However, the orientation has a little different from the analytical solution. Considering the

average direction of propagation has value of $\alpha = 68^\circ$, the calculated value of the groove angle was $\rho = 34.5^\circ$.

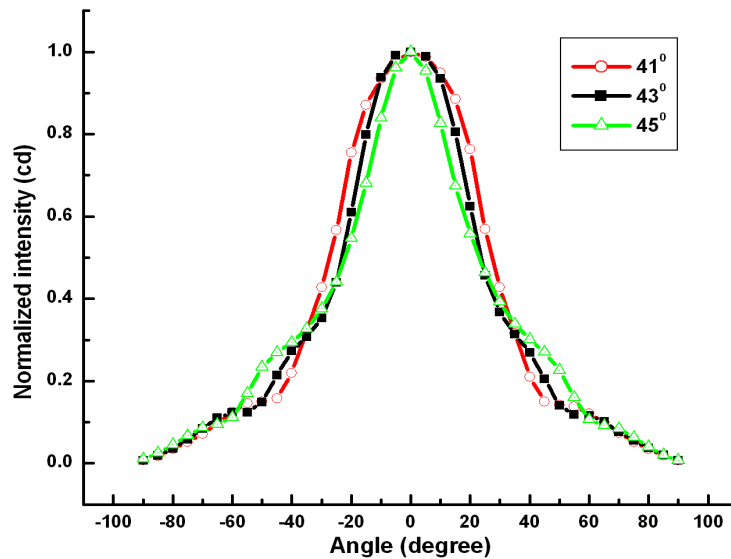


[Fig 3.10] The angular distribution simulated under the various groove orientations

After choosing the proper groove's angle, the uniformity and efficiency should be enhanced with the optimized micro groove distribution. There were two encoding schemes, as illustrated in [Fig 3.11], to be considered. The first approach keeps all the size of the micro groove and modulates the groove spatial frequency along the Z-axis. The other method tends to keep the groove spatial frequency constant and to vary the groove widths along the X-axis and Z-axis. Naturally, the spatial frequency and the groove dimension could be changed simultaneously for the generation of more complex lighting distribution. In this place, the first approach was taken into account for the initial optimization, and then the grooves width w_z along the Z-axis modulated according to the Gaussian function will be discussed.

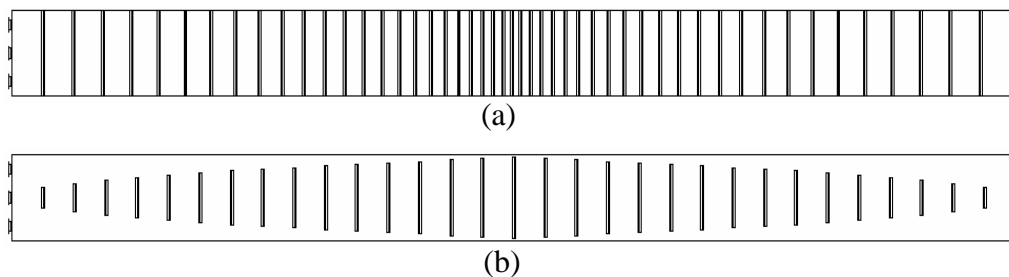


[Fig 3.11] Encoding schemes of (a) modulating frequency and (b) varying groove size

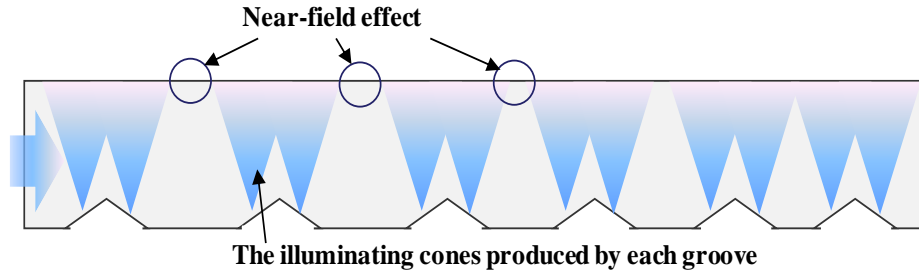


[Fig 3.12] Near-field discontinuities

However, here an indicative criterion should be considered that the maximal groove depth d_{\max} must smaller than the height of the pipe twenty times at least to diminish the visible groove pitches.

$$d_{\max} \leq \frac{\text{The height of the pipe}}{20} \quad (3.1)$$

The smaller groove width also allows producing a smoother illumination distribution. In other words, it can prevent the perturbation in uniformity because of the near-field discontinuities shown in [Fig 3.12]. The initial value of the groove width w_z was chosen as $10\mu\text{m}$, which is capable for the diamond turning fabrication.

By means of the linear decreasing of the groove pitch, the corresponding decreasing ratio for uniformity of higher than 80% for a single pipe was then found. In this optimization process, the groove pitch was varied from 155 to $200\mu\text{m}$ and the decreasing ratio of 0.9995 was determined, where the decreasing ratio was defined as p_i / p_{i+1} (p_i was the pitch between i_{th} groove to $(i+1)_{th}$ groove). As the result depicted in [Fig 3.13], the illumination at the regions marked by the dot line still lower than the other portion and should be improved further.

In order to enhance the illumination at some regions mentioned above and achieve higher uniformity, a Gaussian function was introduced to modulate the grooves width w_z along the Z-axis.

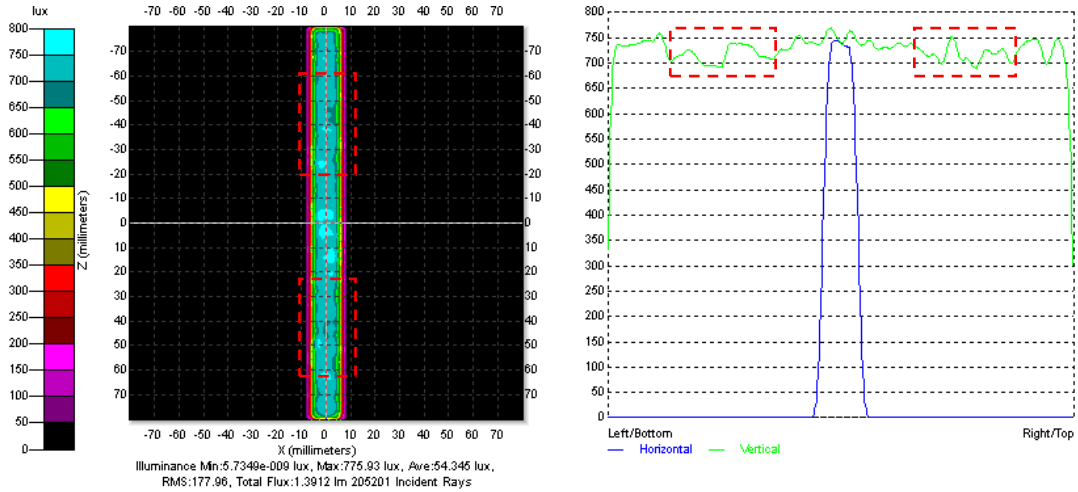


[Fig 3.13] Illumination map of light guide plates with a single division lit up

The Gaussian function is defined as

$$Gau(z) = A \exp\left[-\frac{(z - z_0)^2}{2\Delta^2}\right] \quad (3.2)$$

where z_0 and Δ are the average position and deviation of the Gaussian wave packet respectively, z could be any point along the Z-axis and A means the weighting. The [Fig 3.14] shows two Gaussian wave packets symmetrically arranged and connected at $z_0 = 80\text{mm}$ (the center point of the pipe). The groove width w_z varied from $10.3\mu\text{m}$ to $10.7\mu\text{m}$, which based on the Gaussian distribution with $A=1.07$, $\Delta=20$, and $z_0 = 45\text{mm}$ and 115mm .

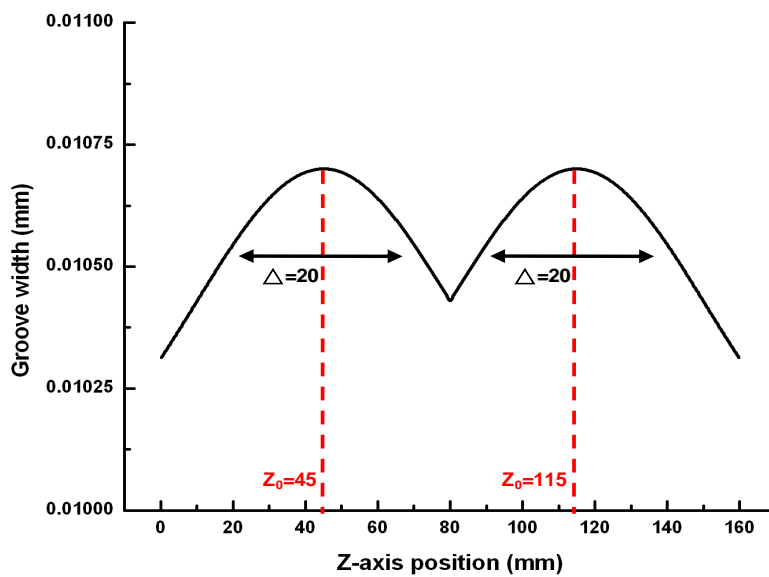


[Fig 3.14] The relation between the groove width and the Z-axis position

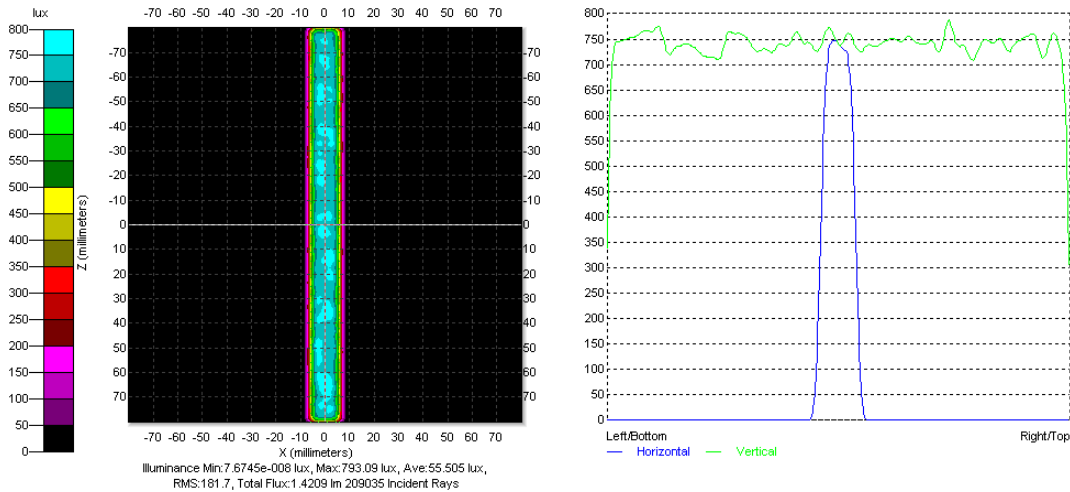


[Fig 3.15] Illumination map of light guide plates with a single division lit up

According to the optimized groove width distribution shown in [Fig 3.14], the simulation result was revealed in [Fig 3.15]. As seen in the figure, the uniformity was indeed improved by the Gaussian function distribution and the angular distribution depicted in [Fig 3.16] is almost the same as that in fixed groove width. The uniformity of higher than 85% and the divergent angle of the extracted light less than $\pm 31^\circ$ on the x-z plane were achieved. In addition, the light leakage from each pipe of light guide to adjacent divisions merely accounted for 3.6%, shown in [Fig 3.17]. However, the total optical efficiency attained only to 60%.

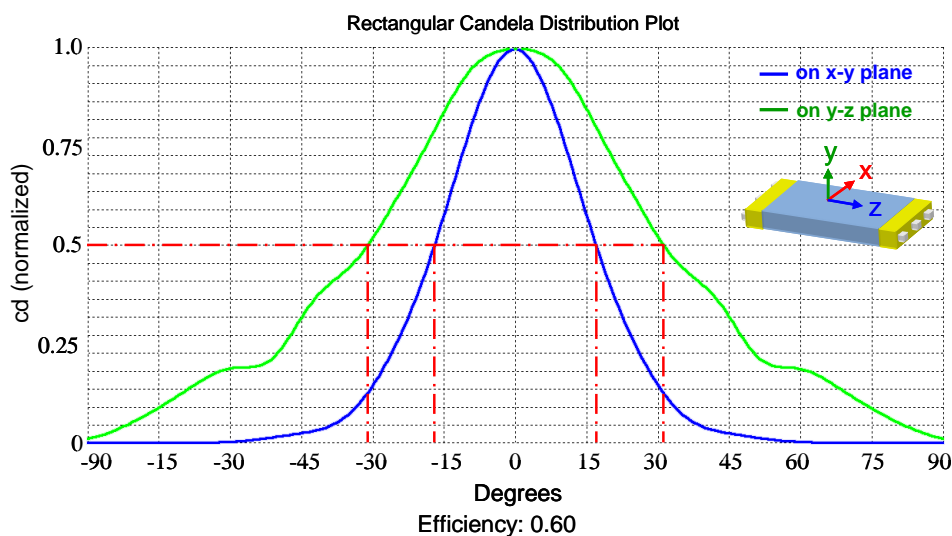


[Fig 3.16] Rectangular candela distribution plot for divergence of light extraction on the x-y and y-z plane, respectively.

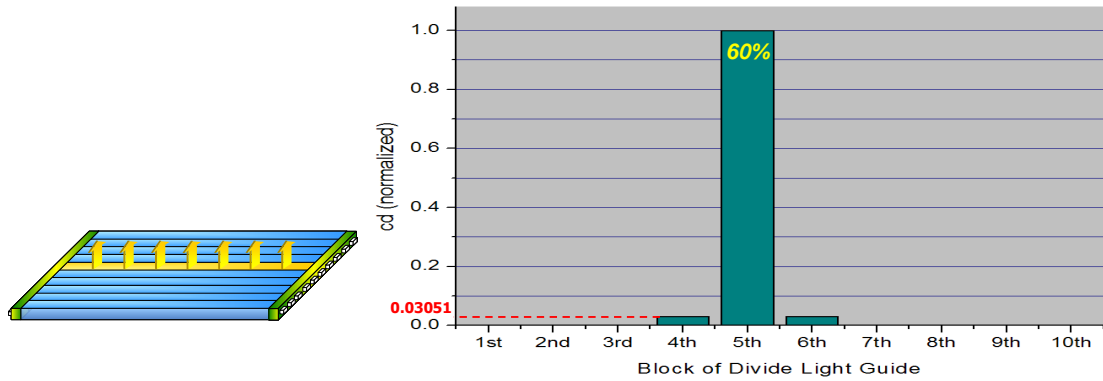


[Fig 3.17] Illumination map of light guide plates with a single division lit up

3.6 Summary

A spatial-temporal scanning backlight for field-sequential-color display system was designed and simulated. The optimal directivity of extraction light occurred in the prism orientation ρ adapted as 43° , meanwhile, the divergent angle of the extracted light less than $\pm 31^\circ$ on the x-z plane were achieved. The color dependence can be considerably diminished in the sequentially driven backlight scheme. The uniformity of higher than 85% was achieved and the light leakage was well suppressed to 3.6%. However, the optical efficiency still has a space to be further improved afterward.

Chapter 4

Experimental Results and Discussions

4.1 Introduction

The field-sequential color backlight system shown in [Fig 4.1] was demonstrated using the light sources of 60 packages of R, G, B, 3-in-1 LEDs. The optimized light pipes with the micro-groove structures arranged on the bottom were fabricated by the diamond knife micro-machining technology. In this chapter, the optical characteristics of the backlight module and the light pipe will be introduced and discussed. In the first part, the integrating sphere was utilized to measure the optical property of the 3-in-1 LED. After that, the fabricated micro-groove structures were examined with the optical microscope and the alpha step. In addition, the Conoscope detected the collimating degree of the illuminating light from the light pipe output surface. Finally, the light leakage from the single lit up light pipe to adjacent light pipe and the uniformity of the whole panel were captured by the CCD camera.

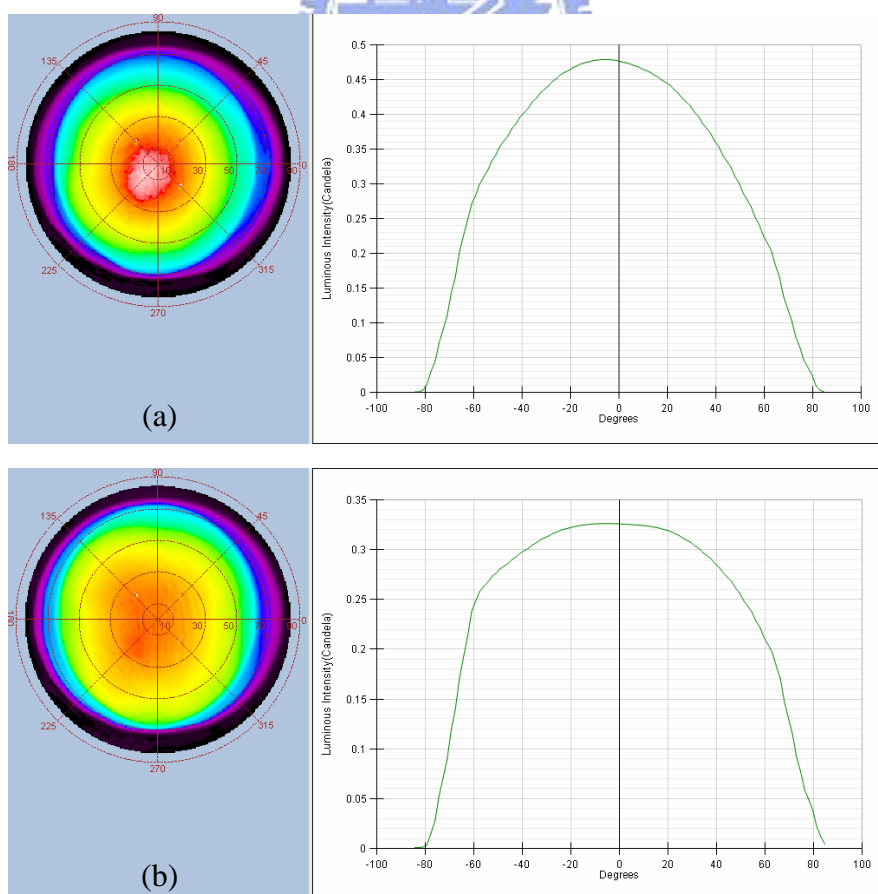


[Fig. 4.1] FSC LCD backlight system

4.2 Light Source Properties

The three packages of LEDs at each end of the linear functional light pipe were used, i.e., one pipe corresponds to six packages. One single package contains a red, green, and blue chip. In the experiment, the chromaticity of the R, G, B LEDs are $(x, y) = (0.7362, 0.2634), (0.1656, 0.7406), (0.1453, 0.0597)$, respectively, that results in a color gamut greater than 120% of the NTSC (National Television Standard Committee) standard. Owing to the color representation of the FSC LCD directly depends on the characters of the light source, i.e. LED, the FSC display usually have better color saturation than the traditional display using the white light source.

In fact, the angular distribution of the LED, shown in [Fig 4.2], has the great influence on the uniformity as well as the angular distribution of the backlight system. The blue and red light angular distributions seem have a little asymmetric and wider than the lambrain type that owing to the package design of the LED.



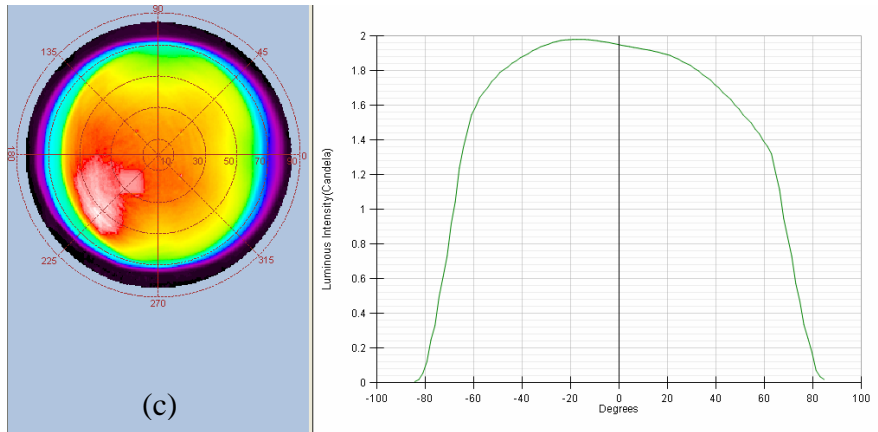


[Fig. 4.2] Angular distribution of the 3-in-1 LED (a) Red (b) Green (c) Blue light

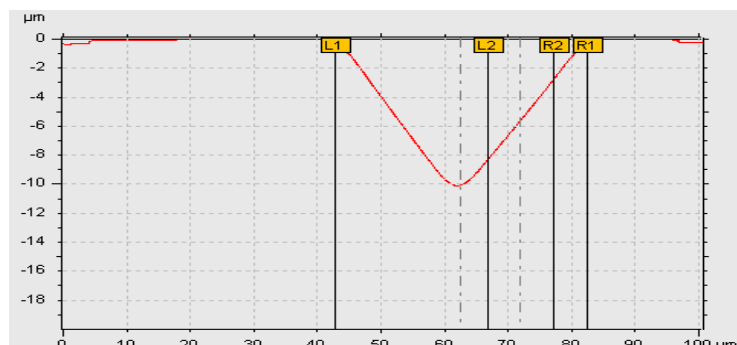
4.3 Micro-groove profiles

The micro-groove structures were manufactured by the diamond knife micro-machining technology supported by the Industrial Technology Research Institute (ITRI). [Fig. 4.3] depicts the micro-groove profiles measured under the optical microscope. The profiles can be observed a little rough and uneven in surfaces where were coated with a thin film Au. The micro-grooves have the same vertex angles of 90° but different pitch size from place to place. However, the rugged on the surfaces can be ignored when the micro-grooves profile without the coating verified by the alpha step as shown in [Fig 4.4].



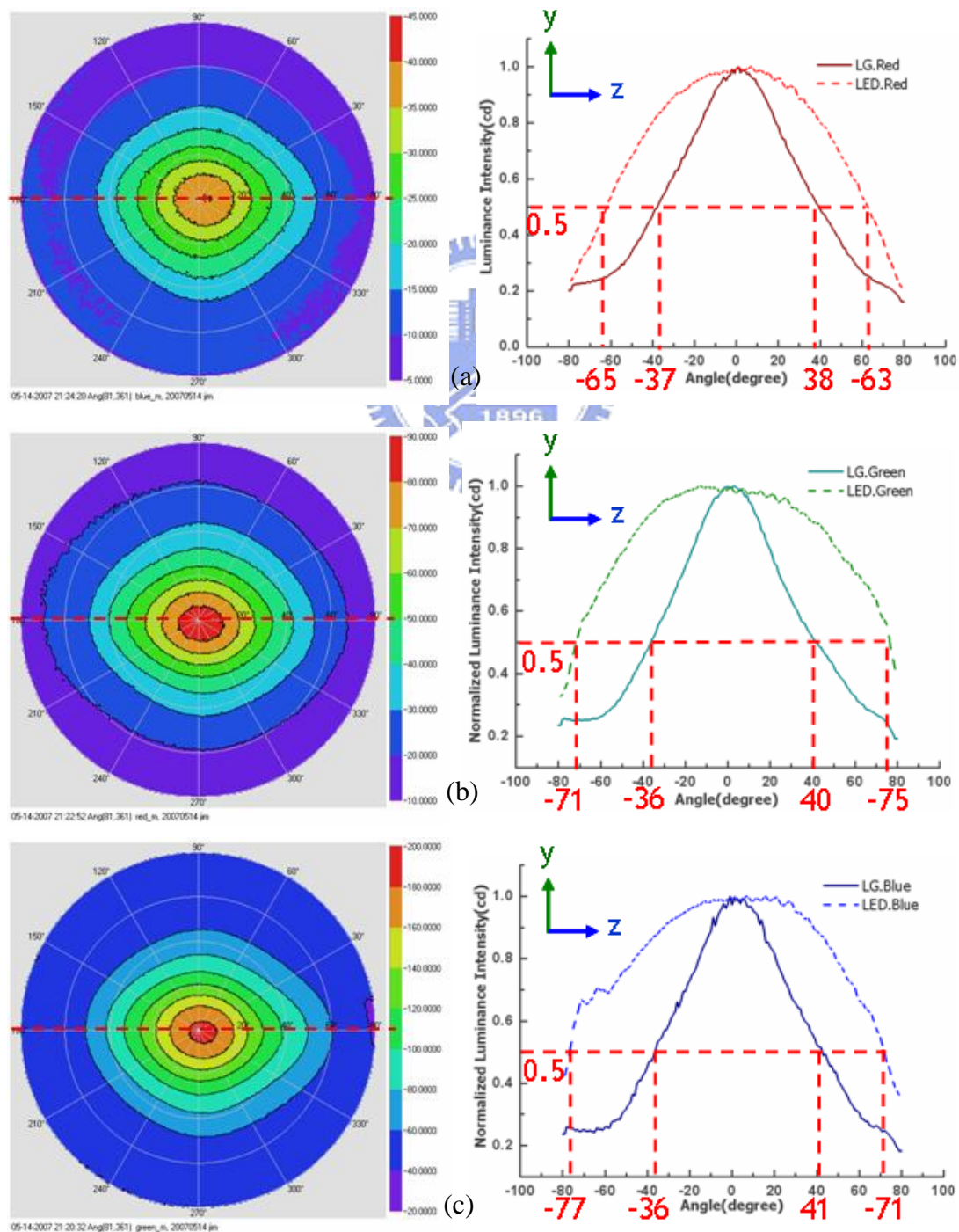
[Fig. 4.3] The micro-groove profiles measured under the optical microscope

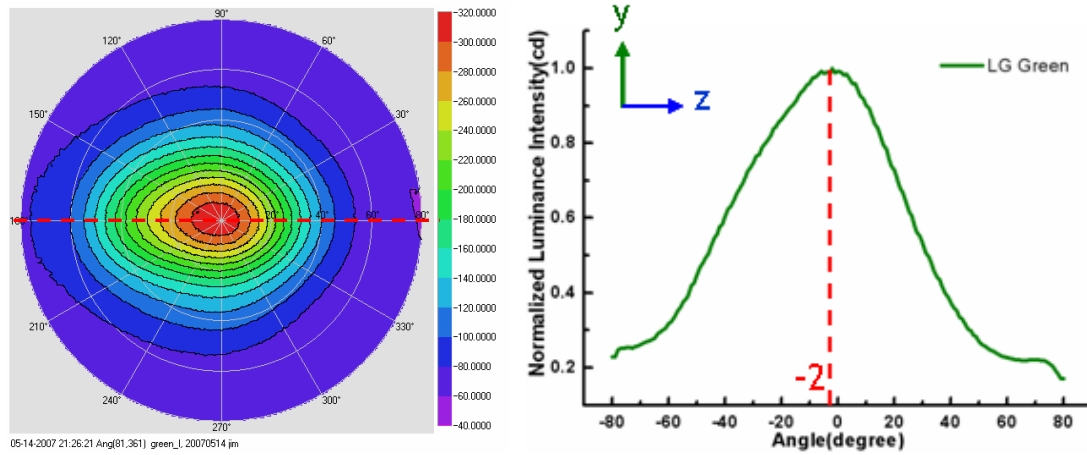
[Fig. 4.4] The micro-groove profiles measured under the alpha step



4.4 Optical Performances

For the whole backlight module, including the ten linear light pipes combined with two light-collimating bars, the optical performances or the optical characters was measured and discussed. A diffuser film was set on the top of the backlight in order to smooth the marked impulse of the illuminating light caused by the micro-groove structure. The angular distribution of the extraction light measured by the Conoscope is depicted in [Fig. 4.5].





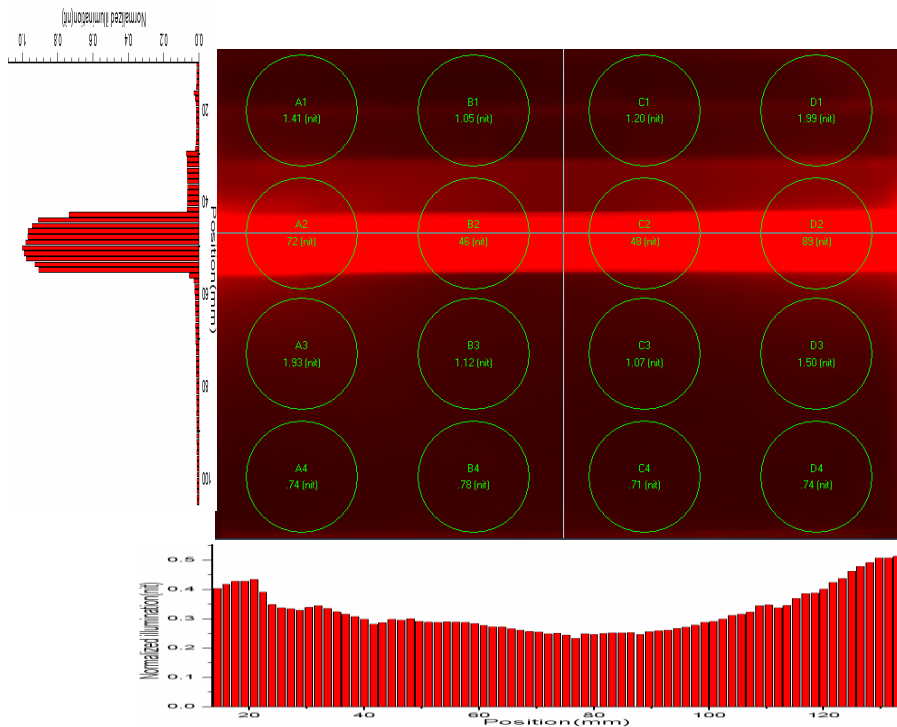
(d) [Fig 4.5] The angular distribution of the extraction light measured at different positions on the light guide output surface: (a) Red light (b) Green light (c) Blue light at center point and (d) Green light at center left point.

The divergent angle of the extraction light for each Red, Green, and Blue color on the Y-Z plane was $-37^{\circ} \sim 38^{\circ}$, $-36^{\circ} \sim 40^{\circ}$ and $-36^{\circ} \sim 41^{\circ}$, respectively. If the reducing ratio for the divergence could be simply defined as

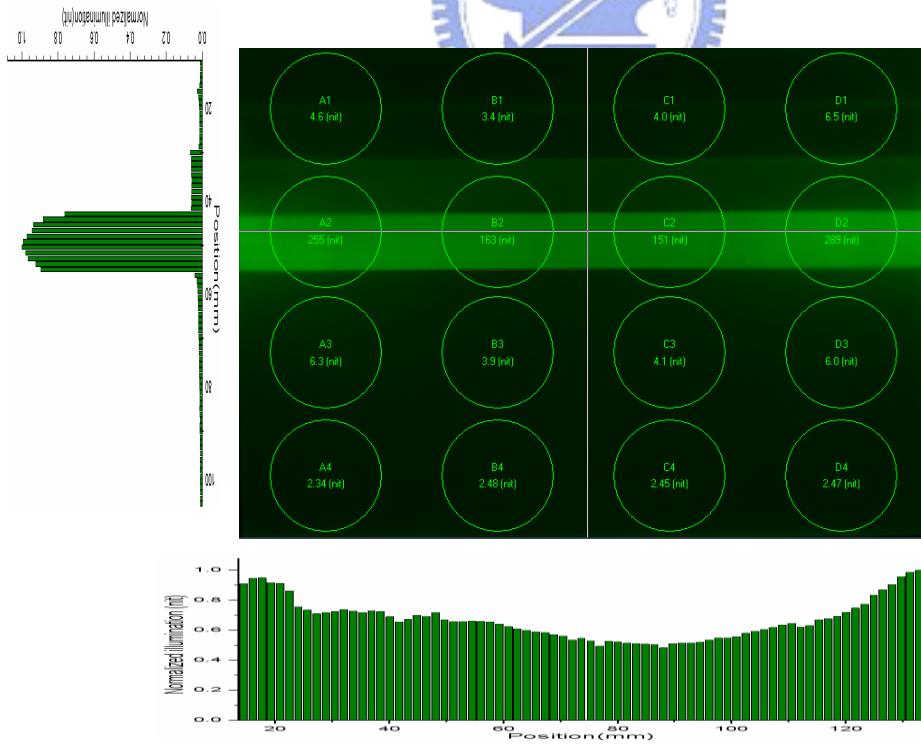
$$\text{Reducing ratio} = \left(1 - \frac{\text{Divergence of the extraction light}}{\text{Divergence of the LED}}\right) \times 100\%$$

there was about 40% ~ 50% reducing ratio from the source to output surface and such high directivity of the extraction light can considerably reduce the occurrence of color dependence for adjacent portions of the light pipe. This characteristic makes the design quite suitable for FSC display. For the measured point strayed from the center point, i.e. the center left point, the whole angular distribution shifted to left side while the peak value deviated 2° from the center point as shown in [Fig 4.5] (d). This phenomenon that the angular distribution has a little change with the different position on the backlight owing to the symmetrical micro structure arranged on the bottom of each light pipe. Therefore, the measured positions close to left side with the shifted distribution due to the left side light source. The uniform angular distribution on each measured point can be obtained by modifying the orientation of the micro structure varied with the distance to the light source. However, the cost rises rapidly at the

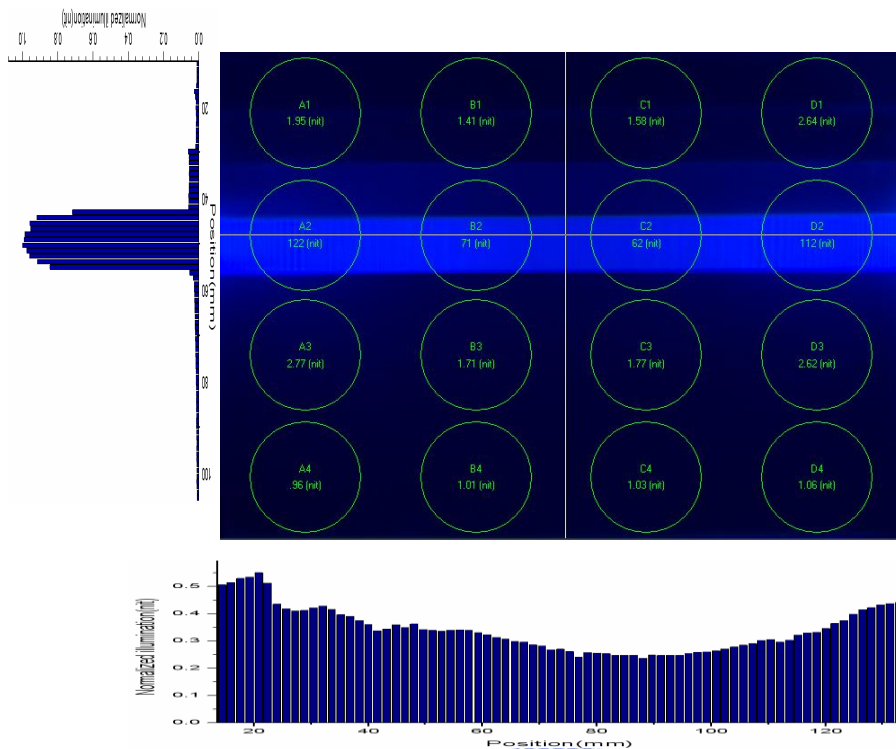
same time.



(a)



(b)



(c)

[Fig 4.6] The sixteen points measurement for the illumination map of light guide plates with a single division lit up: (a) Red (b) Green (c) Blue light.

In order to receiving the uniformity of one block and the light leakage to neighboring divisions, a single pipe was illuminated and captured by the CCD camera. As the results shown in [Fig 4.6], the light penetrate to the adjacent division was well suppressed to below the 7% . For the one distance to three distance division, the light leakage was suppressed to close to zero. There should be no inter-field erroneous color mixture occurred due to this distant light leakage.

So far, the uniformity of a single pipe or the whole backlight only reaches to 55% ~ 60% . Owing to the sensitivity of the human eye, the uniformity should be further improved to fulfill the variation of 20% along the light pipe.

4.5 Summary

The fabricated micro-grooves indeed reduce the divergent angular distribution to a narrow range. There was about 40% ~ 50% reducing ratio from the light source to

illumination surface. Such high directivity of the extraction light can avoid the occurrence of color dependence for adjacent portions of the light pipe. Therefore, the light penetrate to the adjacent division was well suppressed to below the 7% . However, the measured uniformity is not in conformity with the simulation result due to the simplified assumption of the light source, which can be further improved by means of the proper optimization.



Chapter 5

Conclusions & Future Works

Owing to the several advantages such as light weight, power saving and thin volume, the liquid crystal displays (LCDs) turned into more and more popular and has great influence in flat panel displays (FPDs). In the meantime, the image quality of LCD is the critical issue to be extensively discussed by globular researchers and the field sequential color method is expected to be key technology and shall play an important role in the future.

In this study, a prototype of the spatial and temporal scanning backlight system with a 7-inch diagonal size had been accomplished and measured. The developed module was shown in [Fig4.1]. The 3-in-1 LEDs with red, green, blue colors were utilized to generate color fields sequentially in scanning process. The constraint on the light control for each division in scanning backlight was different from that for the ordinary color-filter-type liquid crystal displays. The whole light guide plate consisted of two light-collimating bars and ten functional linear light pipes. Accordingly, the control of light leakage was based on the total internal reflection of the sidewalls of the light pipe. This might resulted in some brighter or darker than the average luminance between two divisions. However, by using the leaked-light emergent from the light pipe and mounting the optical film, the boundary could become more smoothly. The micro-groove structures fabricated by the diamond turning technique and arranged on the bottom of the light pipe were applied to utilize the light energy more efficiently and control the angular distribution of the illuminating light as well as the uniformity along the pipe direction.

In simulation, the functional light pipe was designed and optimized by varying

the micro-groove structures and distribution, including the groove angle, groove width and pitch. The optimized groove angle of 43° with the tolerance of $\pm 2^{\circ}$ had the most narrow divergence angle of $\pm 31^{\circ}$. The groove pitch varying from $155\mu\text{m}$ to $200\mu\text{m}$ and the groove width varied from $10.3\mu\text{m}$ to $10.7\mu\text{m}$ in according to the Gaussian distribution. In addition, the uniformity for a single pipe or the whole backlight of 85% was achieved while the light penetrated to the neighboring pipe could be restricted to 5%.

In the experiment, the Conoscope and the CCD camera were utilized to measure the optical performances of the FSC backlight system. The result shown the angular divergence of $\pm 38^{\circ}$, i.e. reducing ratio of 40% ~ 50% from the source to output part, could be reached. The light leakage to the adjacent division was well suppressed to below the 7%. For the one distance to three distance division, the light leakage was suppressed to close to zero. Accordingly, there should be no inter-field erroneous color mixture occurred due to this distant light leakage. However, due to the simplified assumption of the light source, the uniformity of a single pipe or the whole backlight of only 55% ~ 60% could be attained, which can be further improved by the proper optimization.

In the future, in addition to improve the optical performance of the spatial and temporal scanning backlight system, a complete field sequential color display can be realized by combining the backlight with a optically compensated bend (OCB) mode liquid crystal panel which has fast switching time between gray to gray transfer. Accordingly, the influence of the gap between two divisions and inter-field erroneous color mixture can be judged and some image performances such as motion blur and color breakup can be measured.

Reference

- [1] K. K. Li, *Illumination engine for a projection display using a tapered light pipe*, U.S. Patent #6739726 (2004).
- [2] N. Takahashi and S. Umemoto, *Liquid crystal display apparatus having light pipe with reflective polarizer*, U.S. Patent #6778235 (2004).
- [3] E. Nestler, *Light pipe for an optical mouse*, U.S. Patent #4716287 (1987).
- [4] S. Staley and S. W. Stout, *Eject button for disk drive with light pipe*, U.S. Patent #6717769 (2004).
- [5] A. Gupta, J. Lee, and R. J. Koschel, *Design of efficient lightpipes for illumination by an analytical approach*, Appl. Opt. 40, 3640-3648 (2001).
- [6] J. F. Van Derlofske and T. A. Hough, *Analytical model of flux propagation in light-pipe systems*, Opt. Engr. 43, 1503-1510 (2004).
- [7] S. -C. Chu and J. -L. Chern, *No-loss bent light pipe with an equiangular spiral*, Opt. Lett. 30, 3006-3008(2005).
- [8] Y. -K. Cheng and J. -L. Chern, *Irradiance formations in hollow straight light pipes with square and circular shapes*, J. Opt.Soc. Am. A23 427-434(2006).
- [9] L. R. Daveport, A. Hough and J. Cassarly, *Optimization for Efficient Angle-to-Area Conversion in Illumination Systems*, Proc. of SPIE Vol. 5524 (2004).
- [10] R. J. Koschel and A. Gupta, *Characterization of lightpipes for efficient transfer of light*, Proc. SPIE Vol. 5942 (2005).
- [11] Fumiaki Yamada, Hajime Nakamura, Yoshitami Sakaguchi, Yoichi Taira, *Sequential-color LCD based on OCB with an LED backlight*, JSID, 10/1, 81-85 (2002).
- [12] Kälil Käläntär, Tadashi Kishimoto, Kazuo Sekiya, Tetsuya Miyashita, Tatsuo Uchida, Yoshitami Sakaguchi, Yoichi Taira, *Spatio-temporal scanning backlight mode for field-sequential-color optically compensated-bend liquid-crystal display*, JSID, 14/2, 151-159 (2006).
- [13] T. Uchida, et al., *Color imaging and display system with field sequential OCB LCD*, SID Digest, 13.2, 166-169 (2006)

- [14] Juan Manuel Teijido, *Conception and design of illumination light pipes*, Ph.D. Thesis (University of NeuchÃ¢tel, 1999).
- [15] Akihiro Funamoto and Shigeru Aoyama, *LED backlight system with double-prism pattern*, JSID, 14/11, 1045-1051. (2006)
- [16] KÄlil KÄlÄntÄr, *Modulation of viewing angle on an LCD surface through backlight optics*, JSID, 11/4, 647-652 (2003)

